2020•2021

Faculteit Industriële Ingenieurswetenschappen

master in de industriële wetenschappen: chemie

Masterthesis

Characterization and optimization of the translucent monolithic photoreactors and comparison with other photoreactors

PROMOTOR :

Prof. dr. ir. Mumin Enis LEBLEBICI

BEGELEIDER :

ing. Mathias JACOBS

Jonas Vaes

Scriptie ingediend tot het behalen van de graad van master in de industriële wetenschappen: chemie

Gezamenlijke opleiding UHasselt en KU Leuven

2020•2021

Faculteit Industriële Ingenieurswetenschappen

master in de industriële wetenschappen: chemie

Masterthesis

Characterization and optimization of the translucent monolithic photoreactors and comparison with other photoreactors

PROMOTOR :

Prof. dr. ir. Mumin Enis LEBLEBICI

BEGELEIDER :

ing. Mathias JACOBS

Jonas Vaes

Scriptie ingediend tot het behalen van de graad van master in de industriële wetenschappen: chemie

UHASSELT KU LEUVEN

Acknowledgements

This master's thesis is done to achieve the master's degree in chemical engineering technology. During these studies I have learned a lot and I'm grateful to end this journey with a fun and educational project.

My research would have been impossible without the aid and support of my supervisor ing. Mathias Jacobs. Mathias was always available to answer questions/give insight regarding experiments, processing of data, feedback, etc. His positive attitude motivated me to work hard. In addition, I would like to thank ing. Joris Claes for always being there during the day and making sure of a fun and safe working environment. Joris was always there to answer my questions in the lab, and he took the time to explain and teach me the workings of PIVLab. Also, I would like to thank Marleen Segers for the quick assistance and guidance with the HPLC. Then, I would like to thank ing. Arne Vancleef for lending me a pump when needed and at last, I would like to thank my fellow student Vincent Breukeleers for lending me an extra hand with experiments when needed.

Table of contents

List of tables

List of figures

Glossary

ACN	Acetonitrile
DPA	9,10-diphenylanthracene
FFPM	Fluorescent fluid photochemical microreactor
FPS	Frames per second
HPLC	High performance liquid chromatography
LED	Light emitting diode
LSC-PM	Luminescent solar concentrator based photomicroreactor
PSTY	Photochemical space time yield
RB	Rose Bengal
RTD	Residence time distribution
SDS	Sodium dodecyl sulphate
STY	Space time yield
UV	Ultraviolet
Vis	Visible

Abstract in English

Photochemical reactions have a couple of advantages compared to thermochemical reactions such as lower energy usage, higher selectivity, and access to new reaction pathways. Despite these advantages, photochemical reactions are rarely used in industry due to the limited scalability, caused by the photon and mass transfer limitations. It is hypothesized that a new reactor design can overcome these limitations by utilizing microchannels that are organized in a structured way. This reactor design is known as the translucent monolithic reactor. The purpose of this research is to characterize this reactor and compare it to other photochemical reactors.

The monolithic reactor was characterized by finding its optimal operating point using the model reaction of singlet oxygen with 9,10-diphenylanthracene. This was done by studying the influence of parameters such as light intensity, flow rate, and concentration of the photosensitizer on the conversion, STY, and PSTY. The results at these conditions were compared to the data of a batch experiment and other photoreactors such as the FFPM and LSC-PM. Finally, the first steps towards slug flow within the monolithic reactor were performed.

The monolithic reactor with a conversion of 80%, STY of 1.14 $mmol/l \cdot min^{-1}$, and PSTY of 0.27 $mol/day \cdot kW^{-1}$ was 26 times more productive than the reaction performed in batch but 6.6 times less energy efficient. It also was 20 times more productive and 13 times more energy efficient compared to the FFPM and 6.3 times more productive than the LSC-PM.

Abstract in het Nederlands

Fotochemische reacties hebben een aantal voordelen ten opzichte van thermochemische reacties, zoals een lager energieverbruik, hogere selectiviteit en toegang tot nieuwe reactiewegen. Ondanks deze voordelen worden fotochemische reacties zelden gebruikt in de industrie vanwege de beperkte opschaalbaarheid, veroorzaakt door de beperkingen in de massa en fotonenoverdracht. Er wordt verondersteld dat een nieuw reactorontwerp deze beperkingen kan overwinnen door gebruik te maken van microkanalen die op een gestructureerde manier georganiseerd zijn. Dit reactorontwerp is de translucente monolithische reactor. Het doel van dit onderzoek is de monolithische reactor te karakteriseren en te vergelijken met andere concurrerende fotochemische reactoren.

De monolithische reactor werd gekarakteriseerd door het optimale werkingspunt te vinden aan de hand van de modelreactie van singletzuurstof met 9,10-difenylantraceen. Dit werd gedaan door de invloed te bestuderen van parameters zoals lichtintensiteit, debiet en concentratie van de fotosensitizer op de conversie, STY en PSTY. De resultaten bij deze condities werden vergeleken met de resultaten van een batch reactor en andere fotoreactoren zoals de FFPM en LSC-PM. Ten slotte werd de aanzet gegeven om *slug flow* uit te voeren in de monolithische reactor.

De monolithische reactor met een conversie van 80%, STY van 1,14 mmol/l·min^{-1} en PSTY van 0,27 mol/dag·kW^{-1} was 26 maal productiever dan de reactie die in batch werd uitgevoerd, maar 6,6 maal minder energie-efficiënt. Het was ook 20 keer productiever en 13 keer energie-efficiënter in vergelijking met de FFPM en 6.3 keer productiever dan de LSC-PM.

1. Introduction

1.1. Context

Thermochemical reactions have been used for centuries to convert chemicals. In these types of reactions, the activation energy is delivered by the addition of heat. One of the disadvantages of thermochemical reactions is that unwanted byproducts are formed which must be removed. Furthermore, these reactions are usually energy intensive.

Photochemical reactions are an interesting alternative to traditional thermochemical reactions. In photochemical reactions, the activation energy is supplied by electromagnetic radiation, being photons traveling in a wave-like pattern at the speed of light. Photochemical reactions have a couple of advantages such as lower energy usage, a more selective reaction, a high selectivity, access to new reaction pathways, and a lower to no need for solvents [1], [2].

Both thermochemical and photochemical reactions can be run in flow. Flow chemistry has many advantages in comparison to batch reactions. For example, safety, multiphase reactions, increased heat transfer and the possibility for scale-up. Due to the inefficient utilization of light (Lambert-Beer limitations) and poor heat/mass transfer rates in large-volume in photochemical reactors, batch reactions are difficult to scale-up whereas flow has more potential for scale-up [3]-[5].

To make photochemical reactions viable in industry, high throughputs are desired. For this flow reactors should be used. An example of a photochemical flow reactor is the microreactor. The disadvantages of microreactors are the energy inefficiency and the incapability to handle high throughputs. To improve energy efficiency and throughput, translucent monolithic reactors could be used [6]. A translucent monolithic reactor is a parallel configuration of multiple microreactors made from translucent materials. In Figure 1 a model of a monolithic reactor is displayed.

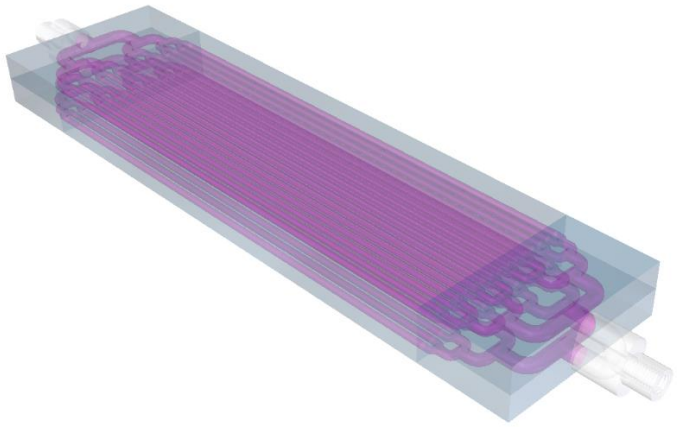

Figure 1: Computer model of a translucent monolithic reactor

1.2. Problem definition / research question

The issue with photochemical reactors is that they are rarely used in industry due to the difficulty to scale up photochemical reactors. Currently no standardized design principles for photochemical flow reactors are reported [7]. Therefore, research is still being done to obtain an optimal design of a photochemical flow reactor. The translucent monolithic reactor is an example of one of these designs. Translucent monolithic reactors have the characteristics of a microflow reactor, and they can facilitate higher throughputs. However, this reactor design has not yet been characterized. To study if the use of translucent monolithic reactors is worthwhile, they must be characterized and compared to other photochemical flow reactors.

1.3. Research objectives

The main research objective of this master thesis is the optimization and characterization of translucent monolithic reactors and compare them to other photochemical reactors. To achieve the optimization and characterization of the monolithic reactors the objective can be split up into **four parts**.

The **first** part is the characterization of the batch and flow reactors (translucent monolithic reactors) with a single-phase reaction. The model reaction for this step is the photocatalytic oxidation of DPA with oxygen forming the endoperoxide of DPA using Rose Bengal as photosensitizer. The **second** part is determination of the RDT for each monolithic reactor for the single-phase reaction. The **third** part to achieve slug flow in the translucent monolithic reactor and make the first steps towards characterizing the slug flow. The **fourth** and final part is the comparison of the obtained results to each other and to available data, such as STY, PSTY of other photochemical reactors found in literature in which it will be determined if the translucent monolithic reactor is better, worse, or equal to these photochemical reactors.

2. Literature study

2.1. Photochemistry

Photochemistry is the study of chemical reactions and physical changes that proceed with absorption of light radiation by atoms or molecules. The absorption of light radiation can excite an electron into a higher molecular orbit, which can cause the breaking of one or more bonds.

An important application of photochemistry is to reduce production costs for chemicals by introducing photochemical steps in the synthesis. Photochemical reactions can lower the production costs because they can be executed under lower pressure and temperature compared to conventional reactions. Moreover, photochemical reactions have access to different reaction pathways that cannot be accessed by thermochemical reactions, potentially lowering the amount of reaction steps needed. Due to the low pressure and temperature, less energy must be put into the reaction. Examples of photochemical reactions are the syntheses of vitamin D, Rose Oxide, Caprolactam. Another application is in the contributions to the ecology, for example, photodegradable plastics [8].

In photochemical reactions, the reaction energy is supplied by the absorption of electromagnetic radiation instead of heat. This makes reaction pathways accessible that cannot be achieved with thermochemical reactions. These different reaction pathways result in different reaction products [9]. The use of photochemical reactions has a couple advantages other than the above-mentioned advantage over thermochemical reactions such as:

- Low energy requirement
- High selectivity
- No/low amount hazardous solvents

There are also specific disadvantages of using photochemical reactions:

- Under- and over-irradiation
- Mass transfer limitations resulting in a slow reaction
- Suboptimal reactor designs resulting in a lower energy efficiency

To get a better understanding of photochemical reactions, the atomic structure and electromagnetic radiation must be discussed.

2.1.1. Atomic structure

Atoms consist of a nucleus made of protons and neutrons orbited by electrons in orbitals. The solution of the Schrödinger wave equation with quantum mechanics shows that electronic energy levels within atoms are quantified. This means that only certain specific electronic energy levels are allowed. Solving the Schrödinger wave equation results in the wavefunctions, Ψ, and their corresponding energies. Ψ^2 provides to the probability of finding the electron at a specific position. This is called the orbital [10], [11].

Three quantum numbers are used to describe an atomic orbital. The first quantum number, the principal quantum number, n, describes the number of electronic shells per atom. As n increases, the atomic orbital will be further away from the nucleus. The further the shell from

the nucleus the higher the energy of the shell will be. Each shell can contain a maximum of $2n^2$ electrons. The second quantum number, the orbital angular-momentum quantum number, *l*, defines the shape of the atomic orbital and can have integer values from 0 to (n-1). The third quantum value, the magnetic quantum number, *m*, describes the orientation of the atomic orbital in space and can have a value of -1, 0 and +1. To get a better understanding on how electrons of atoms arrange themselves into the available orbitals a fourth quantum number must be defined, this is the spin quantum number, m_s. The spin quantum number can have two possible values, +½ and -½. These values indicate to the opposite directions the electron can spin in which the electron can spin, ↑ and ↓ [10], [11].

The Pauli exclusion principle prohibits any two electrons within a given orbital from having the same spin quantum number limiting the number of electrons within that orbital to exactly two. A spinning electron is a moving electrical charge and induces a magnetic field. These spinning electrons with opposite spin in an orbital can be referred to as a singlet [10], [11].

2.1.2. electromagnetic radiation (EMR)

Electromagnetic radiation can be viewed in many ways. In physics EMR refers to the waves of the electromagnetic field, propagating through space, carrying radiant energy [12]. EMR consists of electromagnetic waves, which are synchronized oscillations of electric and magnetic fields as shown in

Figure 2.

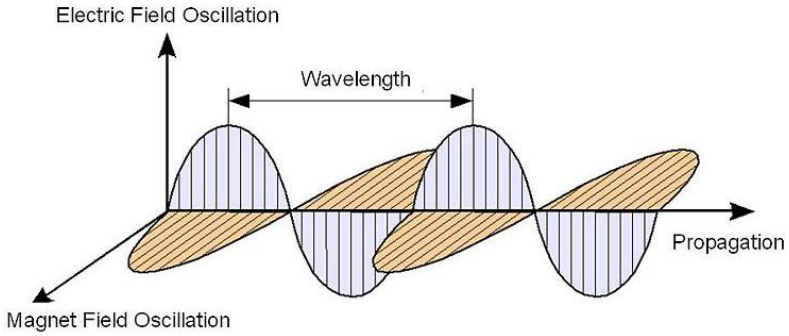

Figure 2: Electromagnetic radiation [13]

In this literature study EMR is viewed as photons, uncharged elementary particles. These photons are responsible for all electromagnetic interactions. The number of photons observed per unit of time is called the photon flux and influences the intrinsic reaction rate of photochemical processes.

The amount of energy a photon can be calculated through the relation between the energy of a photon and its wavelength, this is shown in equation 1 and is also known as Planck's law. The relation between the wavelength and frequency is shown in equation 2.

$$E = h\,f \tag{1}$$

E = The energy of the photons (J)
h = The Planck's constant (6.63 x 10^{-34} J s)
f = The frequency (Hz)

$$c = \lambda f \tag{2}$$

c = The speed of light (3,00 x 10^{8} m/s)
λ = the wavelength (m)
f = The frequency (Hz)

combining equations 1 and 2 gives equation 3:

$$E = h \frac{c}{\lambda} \tag{3}$$

To start a photochemical reaction, electromagnetic radiation is necessary. In photochemical reactions EMR from the ultraviolet (UV)- (10 – 400 nm) and visible (VIS)-radiation (380 – 740) are used. The electromagnetic spectrum is shown in Figure 3.

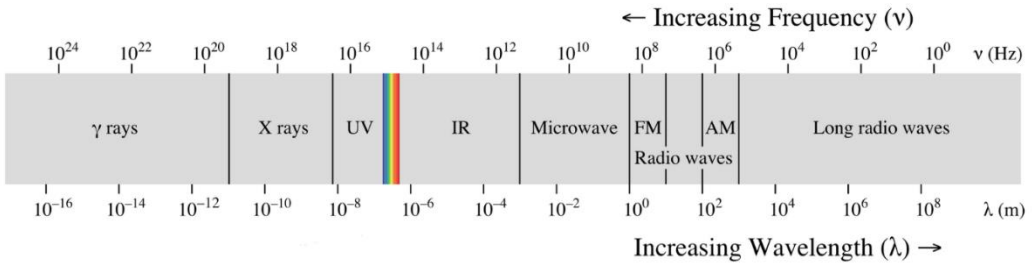

Figure 3: Electromagnetic spectrum [14]

2.1.3. Photochemical reactions

The first step of a photochemical reaction is the absorption of a photon. This induces an electronic excitation that that promotes one of the electrons to an orbital with a higher energy. Such excitation results in the formation of an excited atom. This can result in two different possibilities.

The first possibility is that the two electrons in the orbital with a higher energy have the opposite spins which is referred to as an excited singlet state. The second possibility is that the two electrons have parallel spins which is referred to as an excited triplet state. These states are illustrated in Figure 4.

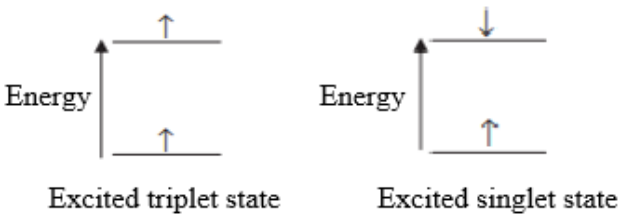

Figure 4: Illustration of excited triplet state on the left and on the right the excited singlet state on the right

Electronic excitation can result in chemical changes. On other occasions, electronic excitation results in deactivation of the excited state by several other physical processes, resulting in the emission of light or conversion of the energy to heat, where the original ground state is reformed. The Excited state can also interact with other ground-state molecules, resulting in energy transfer or electron-transfer reactions provided certain criteria are met [10]. These possibilities for the deactivation of the excited state are also shown in Figure 5.

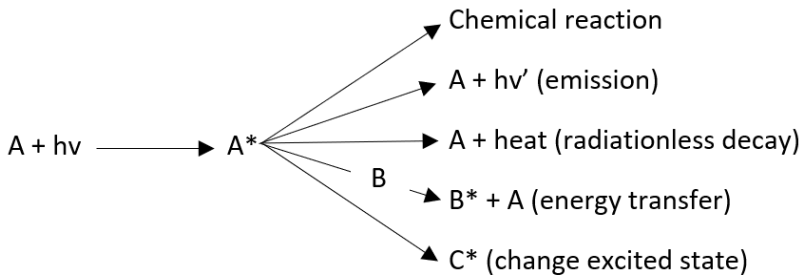

Figure 5: Deactivation possibilities of excited molecules

In absorption of light, a photon that has an equal energy to the energy difference between two electronic states can use this energy to move an electron from a lower energy orbit to the upper one. This produces an electronically excited state. During this process the photon will be destroyed. There are two fundamental principles relating with absorption of light that are the basics for understanding photochemical transformations:

1. The Grotthus – Draper law, states that for light to produce an effect upon matter it must be absorbed [15]. This means that not all light is absorbed by the system.

   Lambert-Beer's law relates the absorption of light to the properties of the material through which the light travels. The absorbance can be calculated through its equation 4.

$$A = \varepsilon \, l \, c \tag{4}$$

   A = The Absorbance
   ε =The molar extinction coefficient (l/(mol cm)
   l = The path length (cm)
   c = The concentration of light absorbing compound (mol/l)

2. The Stark-Einstein law, states that the primary act of light absorption by a molecule is a one-quantum process. This means that for each photon absorbed only one molecule/atom can be excited. There is an exception for this law when using very intense light such as laser. In this case, concurrent or sequential absorption of two or more photons may occur [10], [15].

An important parameter of a photochemical reaction is the quantum efficiency or quantum yield (ϕ), defined in equation 5. The quantum yield can be defined as the amount of product formed over the number of photons absorbed. Most of the times the quantum yield has a value between 0 and 1, and it represents the efficiency of a specific event, in this case a chemical reaction. When the quantum yield equals 1, the number of molecules converted is equal to the number of photons that have been absorbed, resulting in an efficient photochemical reaction without any undesired reactions. The quantum yield can also be higher than 1. This happens when one photon can convert multiple molecules.

$$\Phi = \frac{\#\ molecules\ converted}{\#\ photons\ absorbed} \tag{5}$$

2.2. Reactor design

2.2.1. Batch reactor

A batch reactor consists of a reactor vessel with all reactants needed to perform a desired reaction. First the reactor is brought into the right conditions for the desired reaction and kept there during the process. The reactor is stirred during the entire process. After the process, the reactor is emptied.

Due to the high concentrations of photosensitizer used in photochemical reactions, the majority of the light is absorbed within the first millimeters. This creates dark zones in the reactor, lowering the overall reaction rate. An example of this effect is shown in Figure 6.

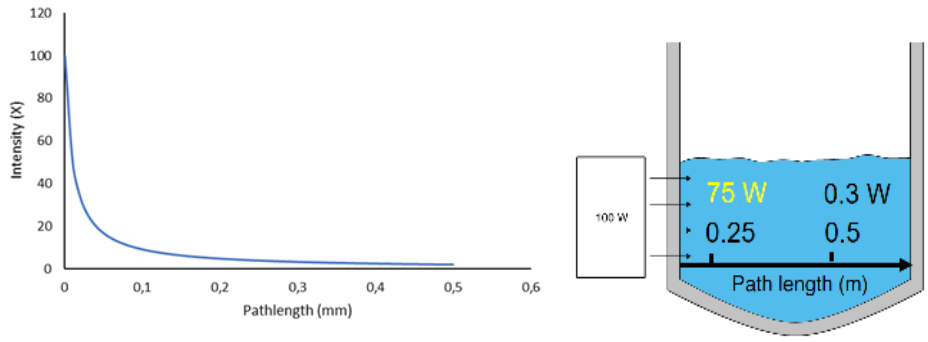

Figure 6: Visualization of the intensity of the light in function of the distance travelled through the reactor

Furthermore, when performing multiphase reactions in a batch reactor, mass transfer from one phase to the other can be the rate determining step, increasing the required reaction time. This is an issue in batch reactors since the interfacial area is low and poorly defined. Also unwanted subsequent reactions can take place because the reactants stay in the reactor [4].

2.2.2. Microreactor

A microreactor is a very small continuous flow reactor. Inside a microreactor there are microscopical channels with a diameter ≤ 1 mm. through which the reagents can flow and react.

The use of continuous flow microreactors for photochemical applications allows to overcome the issues associated with batch photochemistry. A microreactor has narrow channels which provides opportunities to ensure a uniform irradiation of the entire reaction mixture. The

reaction time in a microreactor is also substantially lower which minimizes potential formation of byproducts and results in an increased productivity [4].

Other points of interest of microreactors are the large surface- to volume ratio, mass- and heat transfer characteristics which is important to keep the temperature stable to avoid the formation of unwanted byproducts, enhanced safety, and ease of processing multiphase reaction mixtures.

The most common observed flow pattern in microreactors is laminar as shown in Figure 7. This means that fluid is flowing in parallel layers and mixing is governed by diffusion across parallel lamellae [4]. Mixing is important to prevent the formation of byproducts which originate because of local concentration gradients. This occurs when the mixing time is much larger than the reaction time. In microreactors micromixers are used in which the diffusion distance is minimized to obtain mixing times in the milliseconds range.

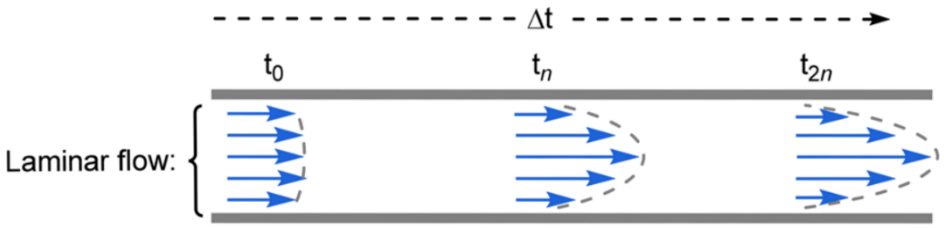

Figure 7: Schematic of laminar flow in a microreactor [4]

One of the major disadvantages of a microreactor is its low throughput due to its small size. A low throughput results in a low amount of product formed during the reaction. Furthermore, the lamps to drive the photochemical reaction are usually too big compared to the microreactor. Therefore, only a fraction of the light is used for the reaction, lowering the energy efficiency. Therefore, both disadvantages are economically unfavorable.

Both disadvantages could be solved with a design as shown in Figure 8, more light can be absorbed by placing channels next to each other and thus forming a 2D reactor. The 2D design can be improved by also placing the channels under each other to absorb even more light, making it a 3D reactor, also called a monolith reactor [4].

2.2.3. Monolith reactor

As mentioned above, a monolith reactor is a 3D reactor with multiple channels next to each other within a single block of material. Usually, monolithic reactors consist out of one piece of material containing many parallel channels. The material out of which the monolithic reactors are either porous catalytic materials or an inert material where catalytic material is coated in the channels. Monolithic reactors were initially developed to clean exhaust gasses from combustion processes both in cars and large power plants. Because they offer a combination of low pressure drop and high surface area. Due to these advantages over conventional reactor types monoliths also have applications in gas-, liquid-, gas-liquid- and gas-liquid-solid phase reactions in different industries [16].

The design of the translucent monolithic reactor will ensure that more light will be absorbed in comparison to the microreactor and thus having a higher energy efficiency. This is illustrated in Figure 8. These monolith reactors also provide the benefits of microreactors, such as high surface to volume ratio and uniform irradiation without suffering from disadvantages such as low throughput [6].

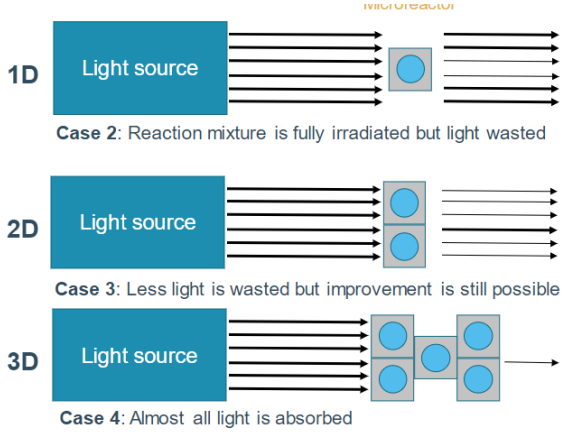

Figure 8: Visualization of light absorbance in 1D-, 2D- and 3D-reactors

There are a couple design parameters in monolith reactors. The channels in a monolithic reactor can be ordered in different configurations such as simple square and square centered. Both are illustrated in Figure 9 with the simple square configuration on the left and the square centered configuration on the right. Other parameters such as the distance between channels and the diameter of the channels can be varied [6].

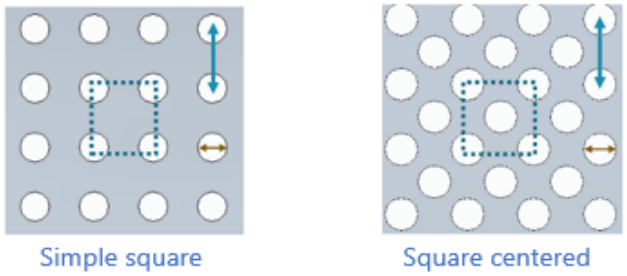

Figure 9: Channel configuration in a monolithic reactor with on the left the simple square configuration and on the right the square centered configuration

2.2.4. Parameters

To optimize a reactor, some parameters can be varied. These parameters are the residence time in the reactor, amount and type of catalysator/photosensitizer and the intensity of the used light to optimize the speed of reaction and conversion.

In continuous flow, the residence time can be increased by decreasing the flow rate and/or by increasing the volume of the reactor. A longer residence time usually results in a higher conversion. The intensity of light can be increased by supplying the light source with a higher energy amount. The greater the intensity of light more reactant molecules are likely to obtain the activation energy and react, making the reaction rate increase due to the greater frequency of initiation.

2.3. Residence time distribution (RTD)

To determine the time particles spend inside the reactor, the residence time distribution graph has to be constructed. This graph is also called the E curve which is the normalized version of the RTD. A typical experiment, to construct the E-curve, consists in sending a nonreactive tracer through the reactor and measure the response. Two experimental methods can be used to construct the E curve. All the equations assume that the used system is considered a closed system [17], [18].

2.3.1. Pulse experiment

First, there is the pulse experiment. In pulse experiments a known volume with a certain concentration of tracer fluid is added to the reactor and the concentration is measured right after the reactor. The concentration is measured in function of time. To normalize this graph and thus construct the E curve, the concentration is divided by the total area under the curve and set out in function of the time. The mean of the C_{pulse} curve can be calculated with the use of equation 6. A visual representation of the transformation from the C(t) to the E(t) curve is given in Figure 10 [17].

$$\bar{t} = \frac{\int_0^\infty tC\ dt}{\int_0^\infty C\ dt} \cong \frac{\sum_i t_i C_i \Delta t_i}{\sum_i C_i \Delta t_i} \tag{6}$$

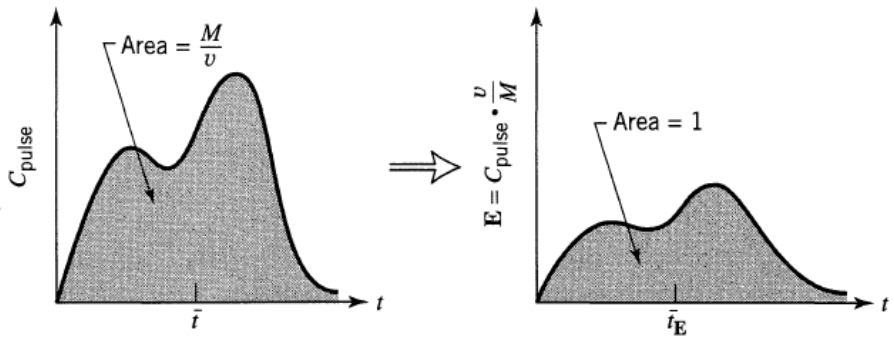

Figure 10: Transformation of an experimental C_{pulse} curve into an E curve [17]

Another RTD function, the E_θ can be used. The E_θ-curve correlates the E-curve to the average residence time. To transform the E to E_θ, the residence time is set out in function of θ = t/$\bar{t}$ and $E_\theta = \bar{t}E$ [17]. A visual representation of the transformation from the E(t) to the E(θ) curve is given in Figure 11.

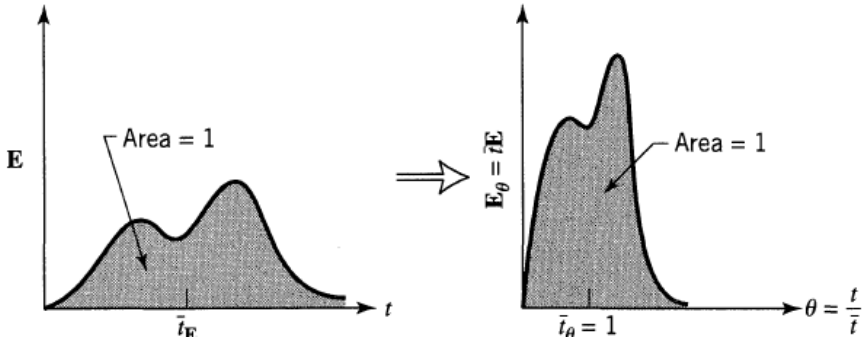

Figure 11: Transformation of an E curve into an E_θ curve [17]

2.3.2. Step experiment

Second, there is the step experiment. In step experiments the fluid is switched to a tracer fluid. The concentration of the tracer fluid is measured right after the reactor. The concentration can be set out in function of the time. To normalize this graph and thus construct the F curve, the concentration should be divided with the highest measured concentration. An example of the F curve is given in Figure 12. The relation between the F and E curve is that $\frac{dF}{dt} = E$ [17].

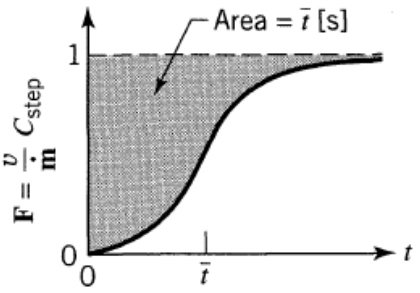

Figure 12: Example of a F curve [17]

2.3.3. Dispersion model

The dispersion model can be used for the representation of flow in real vessels, for scale up, and for diagnosing poor flow. The dispersion coefficient D/uL is evaluated by looking at the RTD-curve. To obtain the value of the dispersion coefficient, the average residence time and the variance on the RTD curve is needed [17].

When the dispersion coefficient is close to zero, a negligible dispersion is observed which translates into plug flow. With larger dispersion coefficients, large dispersion is observed translating into mixed flow. For D/uL < 0.01 equation 7 can be used. For D/uL > 0.01 equation 8 can be used. In Figure 13 the relationship between D/uL and the E_θ curve of the dispersion coefficient is visualized [17].

$$\sigma_\theta^2 = \frac{\sigma_t^2}{\bar{t}} = 2\frac{D}{uL} \tag{7}$$

$$\sigma_\theta^2 = \frac{\sigma_t^2}{\bar{t}} = 2\frac{D}{uL} - 2\left(\frac{D}{uL}\right)^2 * \left(1 - e^{-\frac{uL}{D}}\right) \tag{8}$$

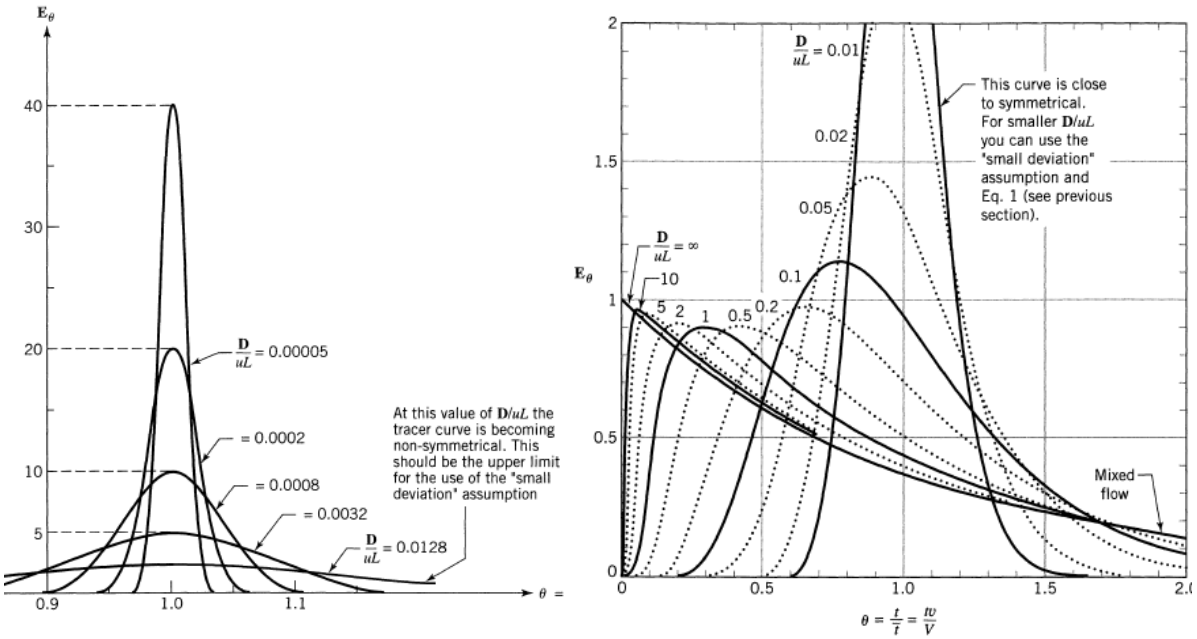

Figure 13: Relationship between D/uL and E_θ curve for small dispersion coefficients on the left and lager dispersion coefficients on the right [17]

2.4. Reaction

2.4.1. Singlet oxygen

Singlet oxygen ($^1O_2$) is a highly energetic, short-lived oxygen species that can be generated by irradiation of a suitable photosensitizers in the presence of triplet oxygen ($^3O_2$), also known as the ground state of oxygen. The molecular orbit of triplet and singlet oxygen are shown in Figure 14. Singlet oxygen can be used for Ene reactions, cycloadditions, or oxidations [4], [5]. With photosensitizers being molecules that produces a chemical change in another molecule in a photochemical process [19]. In other words, photosensitizers are molecules that absorb light in a specific wavelength region depending on their structure. In the presence of oxygen, energy transfer from the excited state of the photosensitizer can occur, yielding singlet oxygen [4], [20].

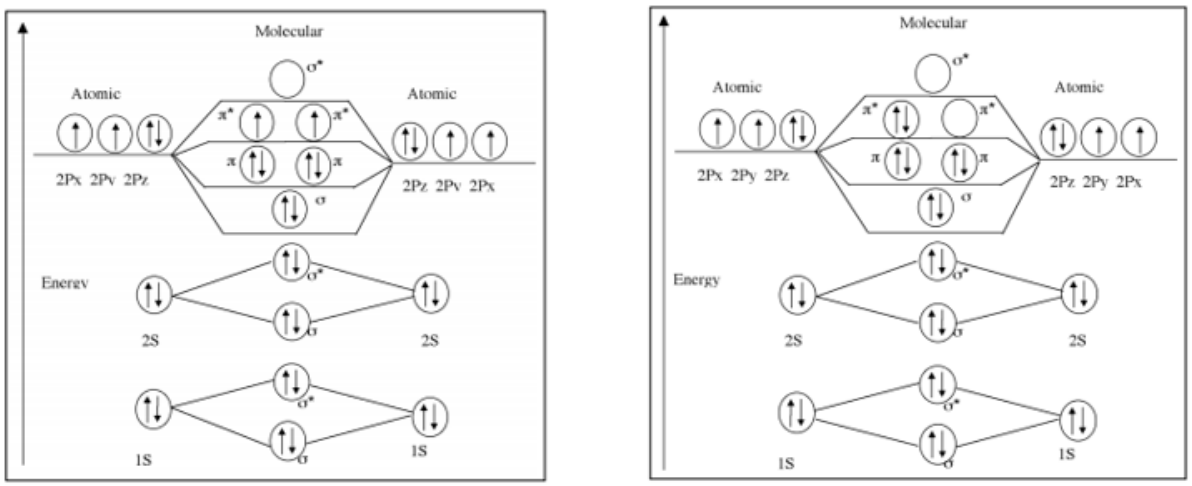

Figure 14: Molecular orbit of triplet oxygen ($^3O_2$) on the left and singlet oxygen ($^1O_2$) on the right [21]

Photosensitizers commonly used for $^1O_2$ generation are methylene blue (MB), rose Bengal (RB), porphyrins such as tetraphenylprophyrin (TPP) and 9,10-dicyanoanthracene (DCA) which, mainly differ in their solubility and absorption spectra in the visible region of light. These photosensitizers with their corresponding λ_{max} are shown in Figure 15 [4], [5].

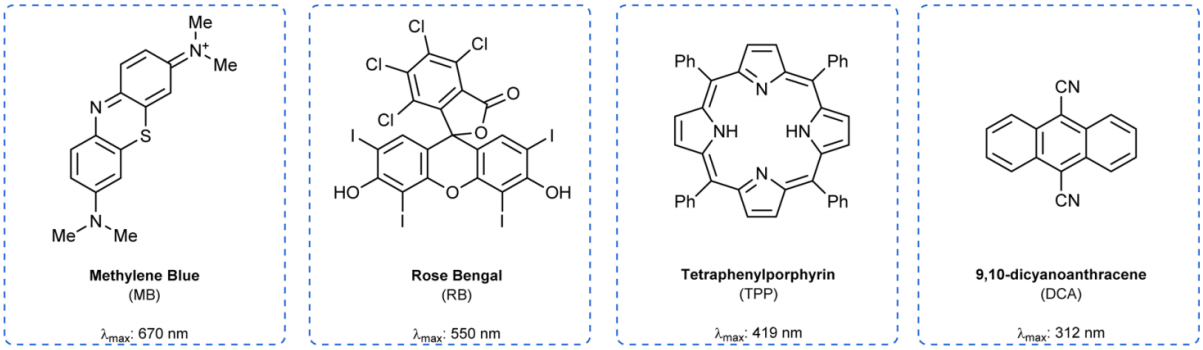

Figure 15: Common photosensitizers for $^1O_2$ generation [4]

2.4.2. The reaction of DPA with singlet oxygen

To characterize the monolithic reactors, a model reaction will be used. This model reaction is the photocatalytic oxidation of DPA with singlet oxygen forming the endoperoxide of DPA. The reaction can also be described as the [4 + 2] cycloaddition of DPA with singlet oxygen. The reaction is shown in Figure 16. This oxidation of DPA is considered a first-order reaction [22]. To excite the oxygen molecules to the singlet-state the photosensitizer Rose Bengal is used.

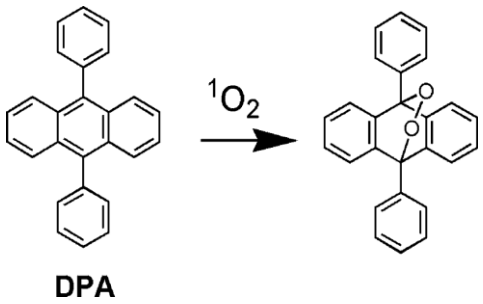

Figure 16: Photocatalytic oxidation of DPA to the peroxide of DPA [23]

2.4.3. Reaction in multi-phase

The photocatalytic oxidation of DPA with oxygen is limited to the amount of dissolved oxygen in the solution for ACN the maximum dissolved oxygen this is 2.42 mM (= 77.44 mg/l) [24]. Therefore, it would be interesting to perform this reaction in gas/liquid multiphase to have a continuous supply of oxygen to the solution.

There are multiple flow patterns within for a gas/liquid system. These flow patterns are annular-, churn-, slug- and bubble flow. These flow patterns are illustrated in Figure 17.

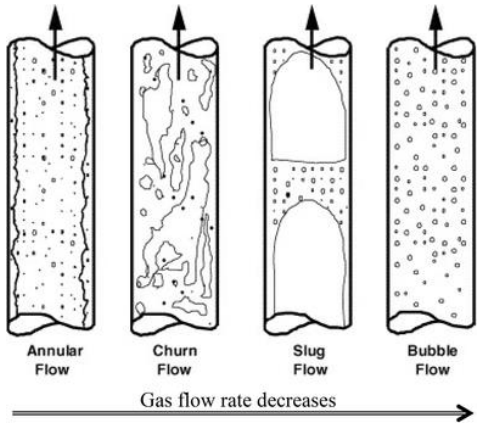

Figure 17: Image of different flow patterns [23]

A map of these flow patterns can be obtained by changing the flowrate of the gas and/or liquid phase and mapping the transitional liquid/gas flow ratio in function of the gas flowrate. An example of a flow regime map is given in Figure 18.

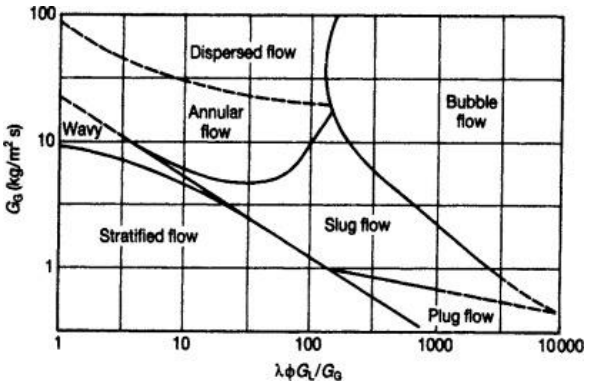

Figure 18: Example map of gas/liquid flow patterns [25]

2.5. Comparison between reactors

To compare the performance of different photocatalytic reactor designs, a solid benchmark is required. In literature two benchmarks are commonly used. The first one is the apparent first order reaction rate constant *k*. This constant gives a direct correlation on the conversion rate. The downside of this benchmark is that it does not give any information on throughput since it is dependent on the volume, light intensity, and photosensitizer load. The second one is the quantum yield, which is mentioned in part 1.3. The disadvantage when using the quantum yield for the comparison between photocatalytic reactors is that the electrical consumption nor the productivity of the reactor are taken into account [26].

Another parameter to compare reactors is the space time yield (STY) and photochemical space time yield (PSTY). STY is a measurement for the productivity of the photocatalytic reaction. The formula to calculate the STY is given in equation 9. PSTY also takes the energy consumption of the light source into account by dividing the STY with the energy consumption [26]. The formula to calculate the PSTY is given in equation 10.

$$STY = \frac{Conversion \cdot C_{start}}{Residence\ time} \tag{9}$$

$$PSTY = \frac{Conversion \cdot C_{start} \cdot Flow\ rate}{Power} \tag{10}$$

2.6. Detection methods

2.6.1. UV/VIS spectrophotometry

UV/VIS spectrophotometry is an analysis technique in which the concentration of a certain substance in a sample to be analyzed is determined by measuring the absorption of visible light (VIS = visible) or of ultraviolet light (UV light). A diagram of a UV/VIS-spectrometer is illustrated in Figure 19.

UV/VIS spectrophotometry can be used to determine the concentration of photosensitizer in the solution by comparing it to a previous constructed calibration curve with known concentrations of the photosensitizer (Rose Bengal).

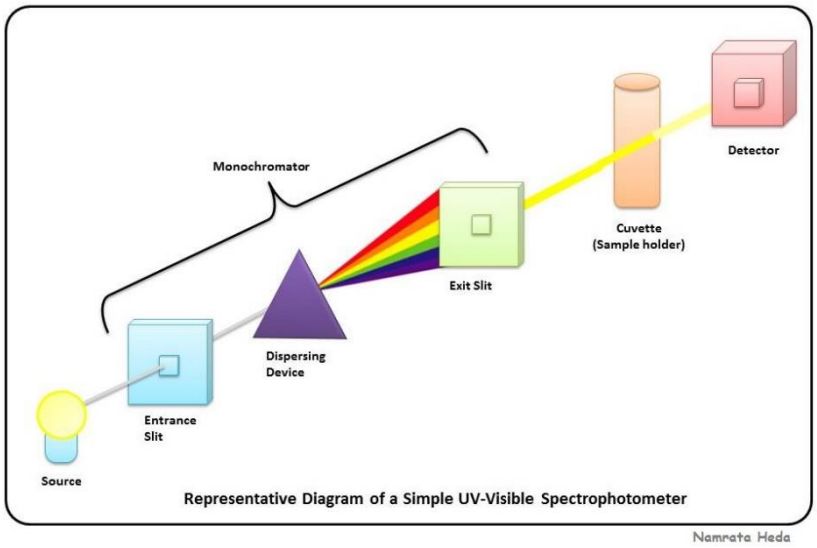

Figure 19: Schematic of UV/VIS spectrophotometry [27]

2.6.2. High-performance liquid chromatography (HPLC)

In HPLC a known volume of sample is injected into a mobile phase also called. This mobile phase is pumped through a column filled with absorbent material being the stationary phase. Each component in the mobile phase interacts different with the stationary phase resulting in a separation of components resulting in a different residence time in the column for each component. After the column, a detector detects these components and registers them with their residence time. And a chromatogram is constructed. The surface under each peak can be determined by integrating them and can be correlated to the concentration of the component at that specific residence time with the use of a previous constructed calibration curve.

HPLC is used to determine the concentration of the reagent DPA in samples. When comparing the concentration of DPA in the sample to the initial concentration in the solution, the conversion, reaction rate, STY and PSTY can be calculated. A schematic of HPLC is shown in Figure 20.

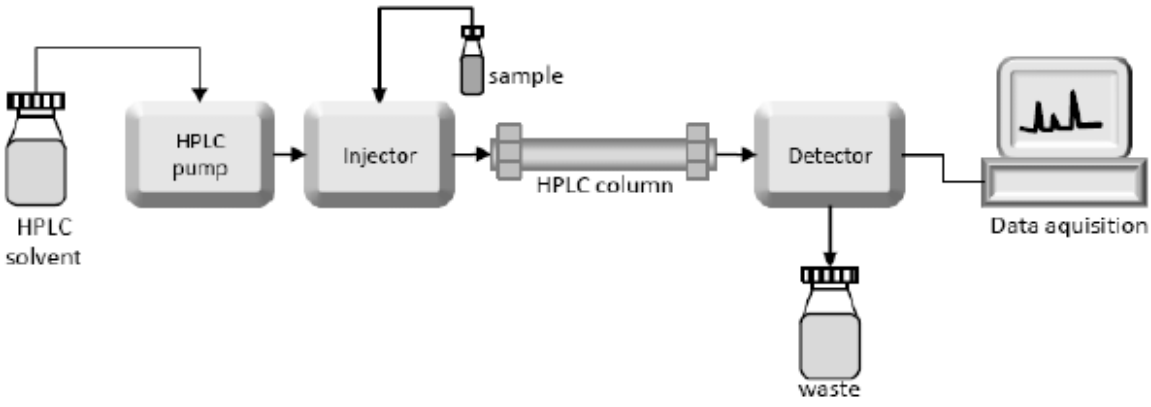

Figure 20: Schematic of HPLC [28]

3. Materials and methods

In this part the experiments that were carried out and the materials used are described in detail. First, the reaction in single phase for the batch and translucent monolithic reactor are discussed. Then, the methods used to achieve slug flow are discussed.

3.1. Single-phase

All single-phase reactions are performed in a darkened fume hood with only the intended LEDs irradiating the reactors. The model reaction that is used is the photocatalytic oxidation of DPA with oxygen forming the endoperoxide of DPA with Rose Bengal being used as photosensitizer. This reaction is also shown in Figure 16. The solvent that is used for the single-phase reaction is ACN containing around 0.5 mM DPA and a varying RB concentration.

3.1.1. Batch reactor

The photocatalytic oxidation of DPA in batch is performed in a continuously stirred 150 ml volumetric beaker with a diameter of 2.75 cm that is covered with a watch glass to minimize the evaporation of ACN during the reaction. The batch reactor contained a 0.5 mM solution of DPA with an optimal concentration of RB calculated with the law of Lambert Beer and is irradiated with a 525 nm, green high-power single LED (SMB1N-525V-02) emitting wavelengths placed approximately 4 cm above the volumetric beaker. The batch experiments are performed at different light intensities by varying the current and at different path lengths. These are respectively 0.1, 0.2, 0.3 A and 10, 30, 50 mm. Another batch experiment without the use of the LED but with the use of environmental light also performed to study the influence of stray light at a pathlength of 10 mm. The samples are taken at intervals throughout 30 minutes to follow the reaction progress within the reactor. An image of the batch setup can be found in Figure 21.

Figure 21: Image of the batch reactor

3.1.2. Translucent monolithic reactor

The photocatalytic oxidation of DPA in flow is performed in four different translucent monolithic reactors. The different dimensions of the translucent monolithic reactors are shown in Table 1 and images of these translucent monolithic reactors are shown in Figure 22. For the reaction, the translucent monolithic reactor is placed in a custom-made dark container within a darkened fume hood to block stray light. During the reaction, the translucent monolith is irradiated with a custom-made water-cooled LED-board consisting out of four LED rows with each 9 LEDs emitting light around 525 nm. The LEDs that are used for the board are high density XLamp XQ-E LEDs from Cree. The translucent monolithic reactors are placed 40 mm from the LED-board.

Table 1: Dimensions of the used monolithic reactors.

Monolith	$d_{channel}$ (mm)	Channels	Length (mm)	Amount of LED rows used
1	1	16x2	150	2
2	1	32x2	150	4
3	2	16x2	150	2
4	1	16x4	150	2

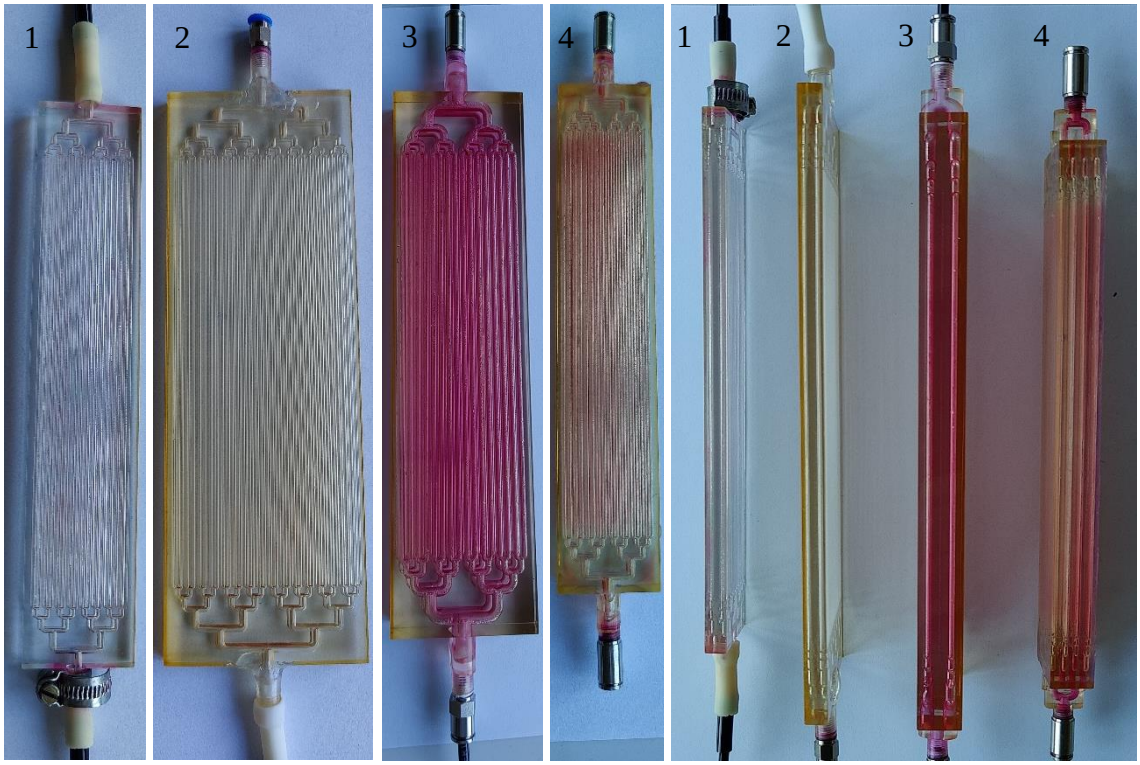

Figure 22: Front- and side view images of all four translucent monolithic reactors

The monolithic reactor is placed straight up with the reagents flowing upwards. Before the LED-board is turned on the reactor is filled up with reagents making sure that flow is achieved in all channels. The used setup can be seen in Figure 23. For this experiment the light intensity, RB concentrations and flow rates are varied. Also, the influence of a reflective background is investigated. The material that was used for this reflective background is aluminum foil. For each datapoint three samples are taken after a runtime of three times the expected residence time.

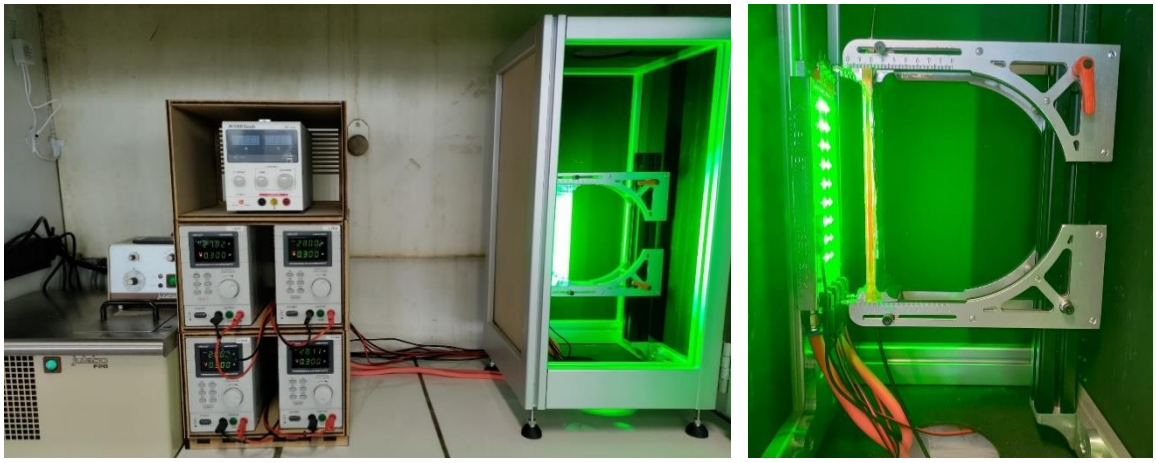

Figure 23: Image of used setup for reactions in flow

3.1.2.1. Residence time distribution

To determine the RTD of each monolith, a pulse experiment is used. The used setup is schematically displayed in Figure 24. In this experiment the reactor is first filled with demineralized water and a fixed amount of 0.1M KCl solution is added by filling the loop with a 0.1 M KCl solution. When operating the valves, so that the KCl solution flows through the reactor the conductivity of the solution can be measured after the reactor using a conductivity monitor. This data is recorded throughout time with the use of Labview software. From the obtained data the RTD curves are drawn, the average residence time, and dispersion coefficient (D/uL) are calculated using the equations from part 2.3.

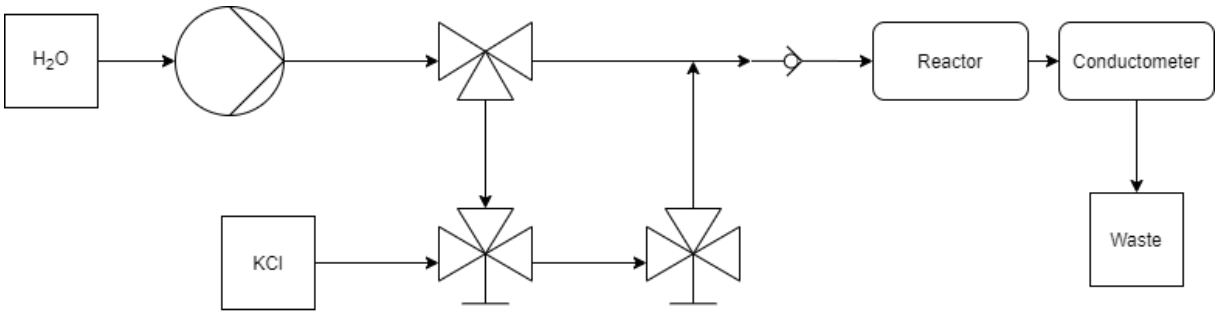

Figure 24: Schematic of used setup for determination of RTD

3.1.3. Data analysis

After taking a sample from the batch- and/or the translucent monolithic reactor the sample is taken in a brown vial that is stored in a dark container to ensure the concentration of the sample stays constant and does not change due to the photocatalytic oxidation. These samples are measured as soon as possible with HPLC. The concentration of DPA is determined with HPLC with a C18 column. The conversion is determined with equation 11. DPA is the only formed reaction product. The settings used in the HPLC method are summarized in Table 2. With this method the following calibration curve is established. In Figure 25 an example of the HPLC chromatogram of a reaction sample is shown.

$$Conversion = \frac{C_{Start} - C_{End}}{C_{Start}} \quad (11)$$

Table 2: Summary of method settings for HPLC

Category	Parameter	Value
Pump	Column flow	1 ml/min
	Stoptime	10 min
	Solvent A (ACN)	95%
	Solvent B (H_2O)	5%
Wavelength detector	wavelength	350 nm
	Reference wavelength	600 nm
	Scan range	190-290 nm
	Scan step	1 nm
Autosampler	Injection volume	20 µl
	Draw speed	100 µl/min
	Eject speed	100 µl/min
Column thermostat	Temperature	Ambient temperature

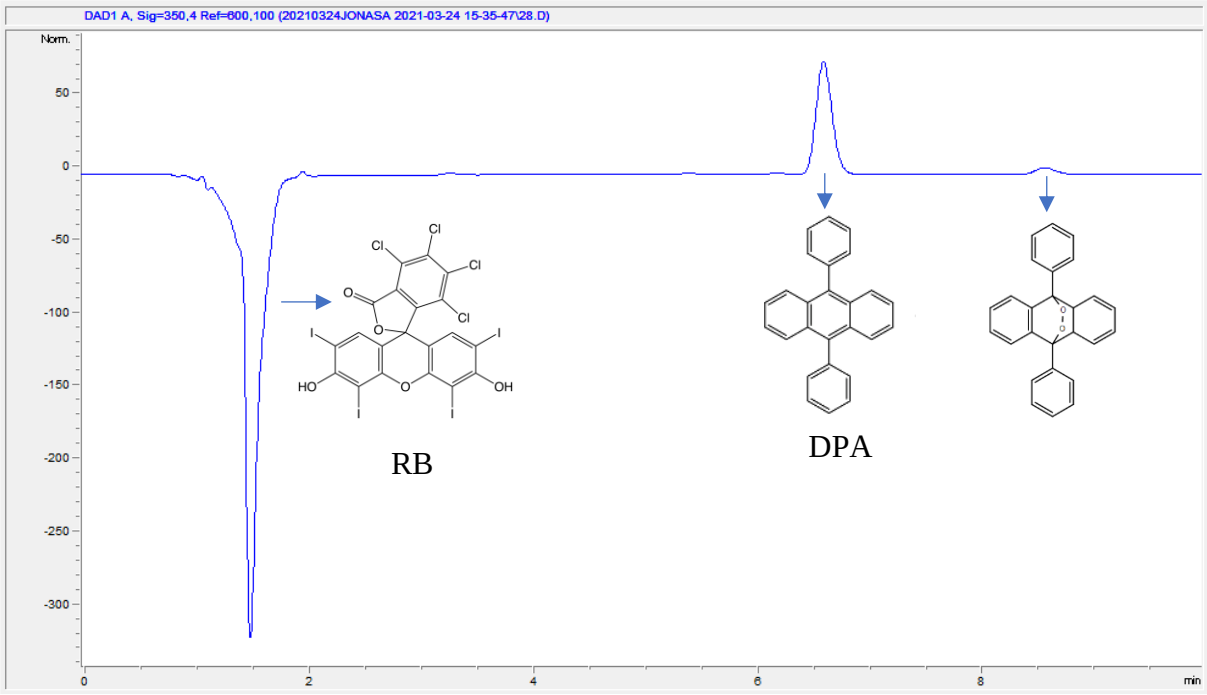

Figure 25: Chromatogram of reaction sample with molecules at each peak

Figure 25 shows 3 peaks in the chromatogram of the reaction solution. The first peak at a retention time of 1.75 minutes is the peak of RB. This peak is negative due the high absorption of RB at a wavelength of 600 nm on which the reference has been taken. The chromatogram of the reference is deducted from the chromatogram at 350 nm to minimize background noise. This is not an issue since the concentration of RB is not measured via HPLC. The second peak that can be seen at a retention time of 6.8 minutes is from DPA. The area of this peak is determined using integration. The area is correlated to the concentration DPA in the sample using the calibration curve shown Figure 26 out of which the conversion can be calculated. The final peak at a retention time of 8.5 minutes is from the endoperoxide of DPA. This peak is relatively small due to the smaller absorption of light at a wavelength of 350 nm. It is mostly used to verify if reaction has occurred.

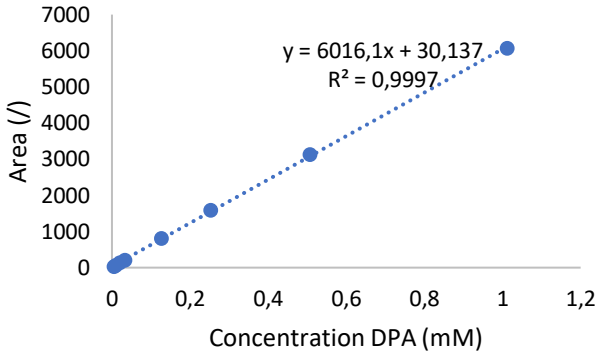

Figure 26: Calibration curve of DPA in ACN

The calibration curve shown in Figure 26 is sufficient to use to translate the areas obtained from the HPLC peaks to concentrations. A repeatability of 0.85 µM is found.

3.2. Multi-phase (G/L)

3.2.1. Steps towards slug flow

The second goal of this thesis is to achieve a gas/liquid slug flow within the translucent monolithic reactor. For the first experiments a piston pump was used to supply the liquid phase and a peristaltic pump was used to pump the gas phase (air). In Table 3 the differences in experiments are shown in the order that they were performed to achieve slug flow.

Table 3: List of experiments carried out in the steps towards slug flow

Experiment	Liquid phase	Flow direction	Additional information
1	Water	Vertical upwards	
2	Water + surfactant	Vertical upwards	0.08 M SDS (surfactant)
3	Water + surfactant	Vertical upwards	Pressure increase after monolith with the use of 0.57 mm tubing
4	ethanol	Vertical upwards	
5	ethanol	Vertical upwards	Switch to a monolith with square channels
6	ethanol	Vertical downwards	16x2 Monolith with square channels, cross section = 1mm^2
7	ethanol	Vertical downwards	Switch to syringe pumps for constant flow
8	Water, water + surfactant	Vertical downwards	
9	ethanol	Vertical downwards	Monolith with square channels, a slit in between 2 rows of channels, and a smaller distributor with channels of 1mm

For experiment 7 and 9 the particle image velocimetry (PIVlab) tool with graphical user interface (GUI) is used in Matlab to visualize the flow rate within the monolith. This is done by recording the slug flow in 480 or 240 FPS and then uploading it to the PIVlab tool and

processing the data to achieve a flow rate chart. The settings that were used for image pre-processing were CLAHE with a window size of 20 px, Wiener2 denoise and low pass at a window size of 3 px, and auto contrast stretch enabled. For the PIV settings the FFT window deformation algorithm was used for 1 pass. The interrogation area and step size has to be found for each experiment and is dependant on the velocity of the moving particles and the amount of frames it was recorded in. After processing the data, the vectors are validated by applying a standard deviation filter with a threshold of 3·stdev.

3.2.2. Multiphase reaction

At last, one multiphase flow experiment is carried out with ethanol as solvent instead of ACN. A 50/50 liquid to air ratio is used at combined flow rate of 30 ml/min. The used setup is almost identical to this of the single-phase flow reaction. The differences are that a 16x2 monolith with square channels with a cross section of 1 mm^2 is used and that syringe pumps are used to pump the liquid and gas solution. The concentration RB and DPA in the reaction mixture are respectively 300 µM and 0.5 mM.

4. Results and discission

The results obtained during this study are presented and discussed in this chapter. This chapter is divided into three parts. First, the single-phase reaction in batch and in the translucent monolithic reactors. Second, the steps towards gas/liquid slug flow within the translucent monolithic reactor. And finally, the comparison of the obtained data to this of other photoreactors.

4.1. Single phase

4.1.1. Batch reactor

As described in the materials and methods section the single-phase batch reaction is performed as a blanco (without the use of an LED), at different pathlengths, and at different light intensities by varying the current to the LED.

Blanco batch reaction

First, the batch experiment is performed with the use of environmental lighting from the surroundings. The conversion graph in function of time is shown in Figure 27.

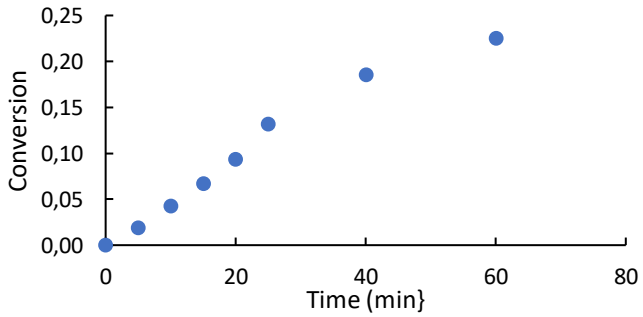

Figure 27: Conversion in function of time for the blanco experiment

In Figure 27 a rising conversion can be seen through time with a conversion of 0.24 after 60 minutes. It can be concluded that environmental light affects the reaction of the photocatalytic oxidation of DPA. Therefore, it is important that all the following reactions are performed in dark areas in which only the intended light source triggers the reaction. This is done by darkening the fume hood, using dark bottles for reagents and samples, and non-translucent tubing. samples are preferably stored inside a dark container for short periods of time to obtain representable results.

Influence of Pathlength

The effect of the pathlength on the conversion, STY and PSTY throughout the residence time in the batch reactor is shown in Figure 28.

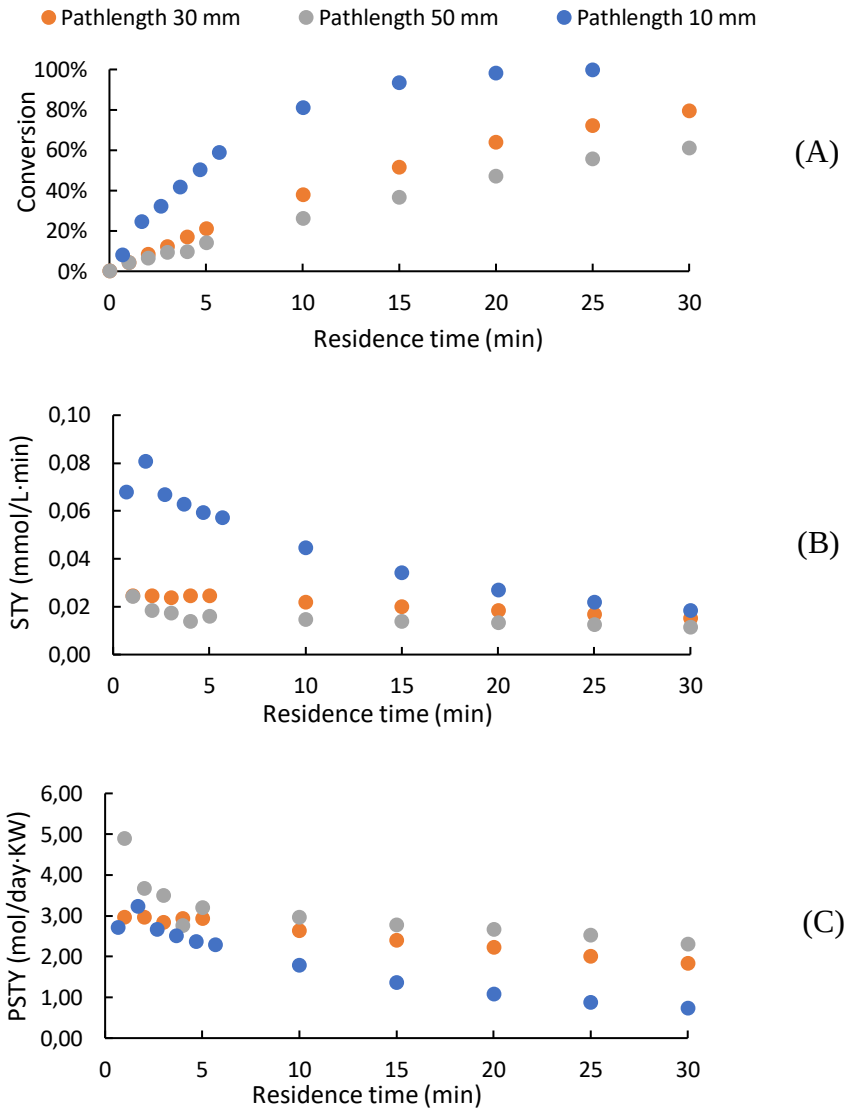

Figure 28: Plot of respectively the conversion (A), STY (B), and PSTY (C) in function of the residence time within the reactor at a current of 0.3 A to the LED at a path length of 10 mm (blue), 30 mm (orange), and 50 mm (grey)

It is shown in Figure 28 that an increase in path length results in a decreased conversion and STY and a PSTY increase. These results are as expected. For each pathlength, the concentration of photosensitizer was calculated to absorb 95% of the incoming light with using the law of Lambert Beer. Resulting in the same amount of light usage for both the large and small volumes. Therefore, higher conversion, higher STY, and smaller PSTY values are expected at shorter pathlengths. Resulting in more reactions taking place per volume at shorter pathlengths and thus higher conversions and STY. For each pathlength the LED uses the same amount of power. In combination with a slightly higher mol amount of DPA reacted the PSTY of larger pathlengths is higher.

Out of these results it is clear that the possibilities for scale-up of batch reactors are limited due to the limitations of the size of the reactor due to the decrease of productivity with an increase of the distance the light has to travel through the reaction mixture.

The effect of light intensity on the conversion, STY and PSTY is shown in Figure 29. The effect of the current is similar at different pathlengths, so only the results at pathlength 30 mm are displayed.

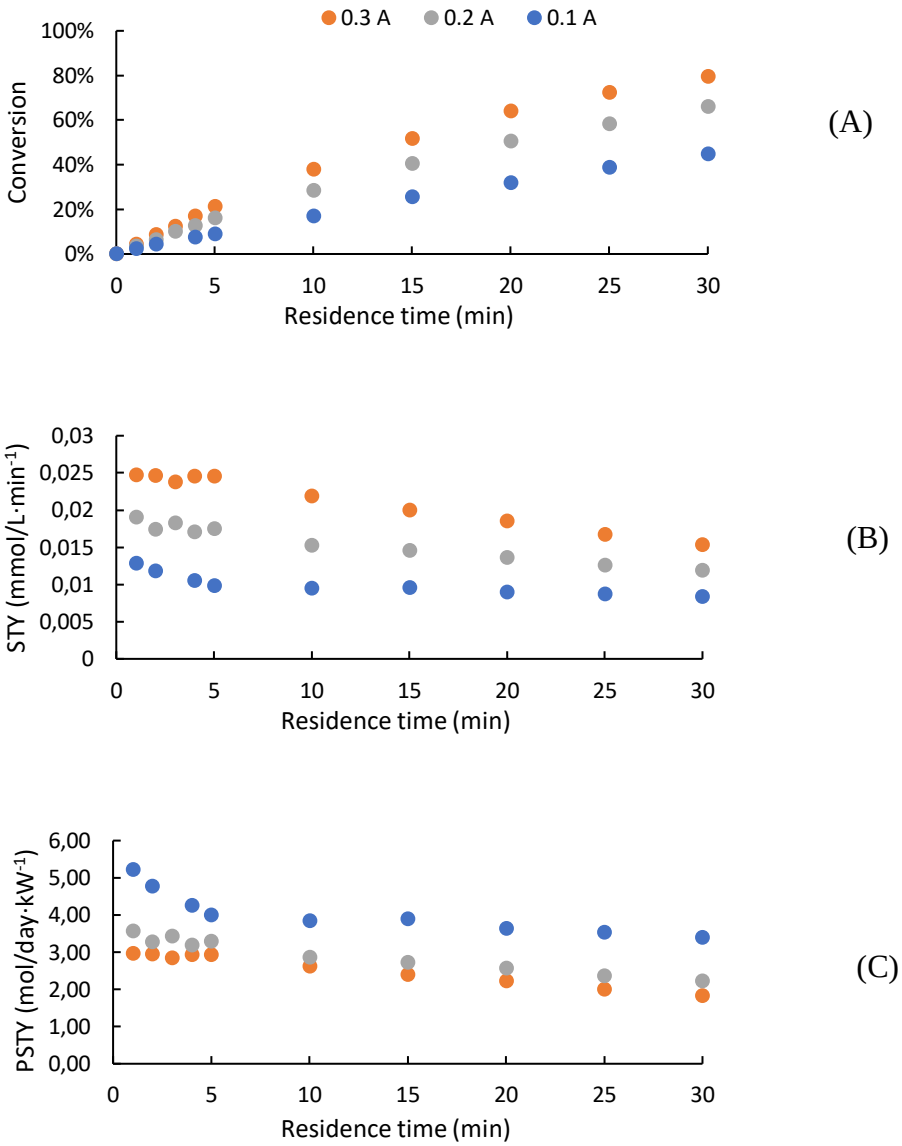

Figure 29: Plot of respectively the conversion (A), STY (B), and PSTY (C) in function of the residence time within the reactor at a path length of 30 mm at a current of 0.1 A (blue), 0.2 A (grey), and 0.3 A (orange)

It is shown in Figure 29 that a higher light intensity results in a higher conversion and productivity (STY). Due to the higher intensity of light, more DPA reacts, and the power used by the LED increases. Both effects counteract each other but the increased power to the LED overpowers the effect on the PSTY. This makes the use of a lower current more energy efficient when only looking at PSTY. When also taking conversion into account, higher conversions are usually more desired due to the lower cost of purification at the end of a process. The costs saved on purification usually outweigh the extra costs of power to the LED.

4.1.2. Translucent monolithic reactor

The single-phase reaction is also performed in the translucent monolithic reactors. First, the RTD for all four monoliths was determined. Then, the effect of a reflective background on the monolith was studied and the optimal operating conditions were determined. Finally, the translucent monolithic reactors are compared to each other to determine which dimensions are most beneficial.

4.1.2.1. Residence time distribution

For each monolith the RTD was determined with a pulse experiment. In Figure 30 the E(t) and E(θ) curves are shown for each monolithic reactor at different flow rates. Table 4 shows the observed residence time, the calculated residence time, and the dispersion coefficient $\frac{D}{uL}$.

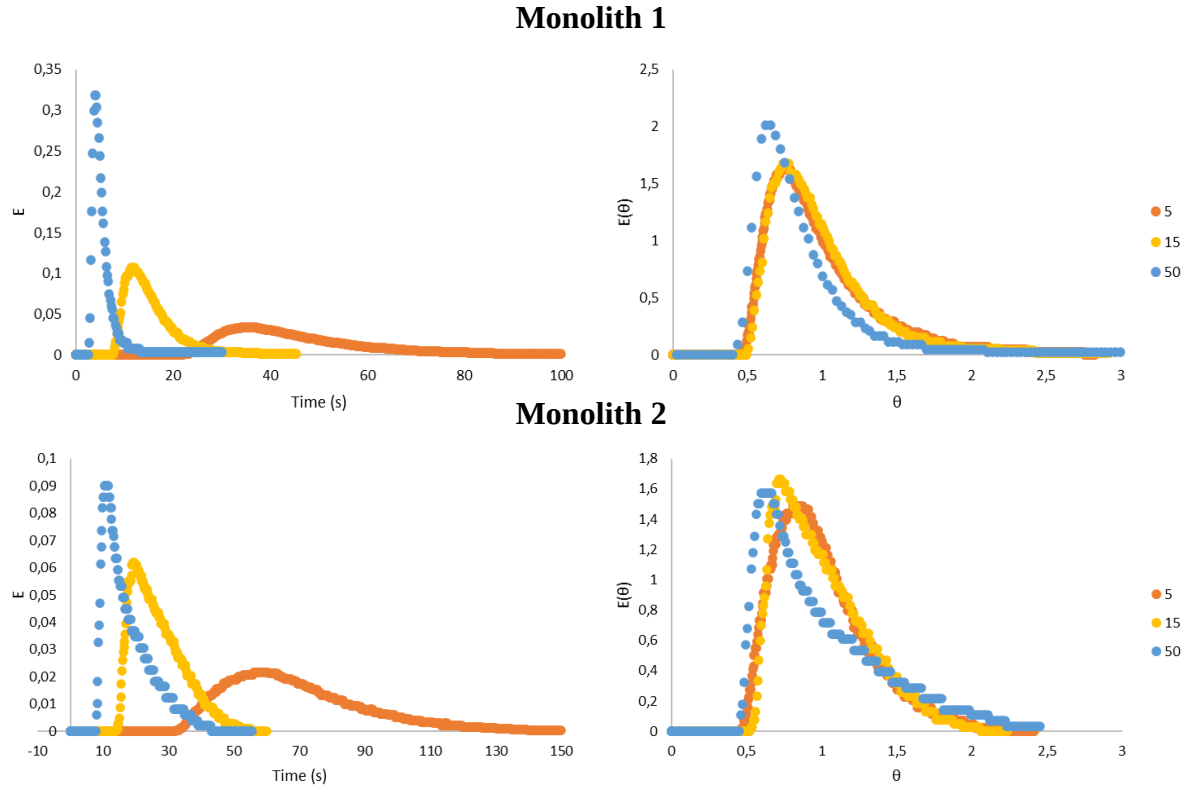

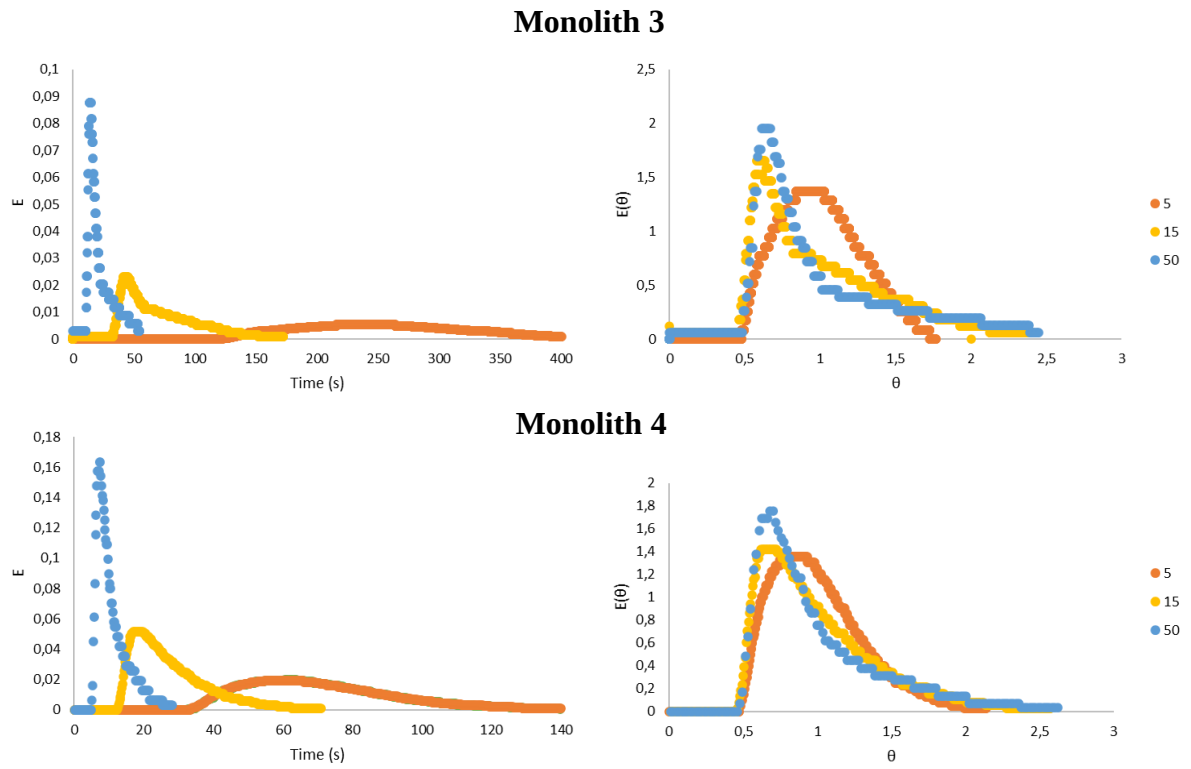

Figure 30: RTD for all four monoliths at a flow rates of 5 ml/min (orange), 15 ml/min (yellow), and 50 ml/min (blue) E(t)-curves on the left and E(θ)-curves on the right.

Table 4: Expected residence time, observed residence time, and dispersion coefficient for each monolith at different flow rates.

Monolith	Flow rate (ml/min)	$\bar{t}_{expected}$ (s)	$\bar{t}_{observed}$ (s)	Difference ($\bar{t}_{expected} - \bar{t}_{observed}$)	$\frac{D}{uL}$
1	5	51.61	47.47	4.14	0.138
	15	18.70	15.57	3.13	0.148
	50	5.86	6.32	-0.46	0.117
2	5	113.12	69.17	43.95	0.153
	15	40.99	26.84	14.15	0.174
	50	12.85	17.47	-4.62	0.104
3	5	226.36	257.07	-30.71	0.159
	15	82.02	71.56	-10.46	0.093
	50	25.72	22.29	3.43	0.130
4	5	104.45	71.01	33.44	0.132
	15	37.85	27.56	10.29	0.117
	50	11.87	10.73	1.14	0.138

Based on the results shown in Figure 30 and Table 4, the following observations can be made. First, all curves are non-Gaussian, the curves all have an elongated tail. A likely explanation for this would be longitudinal backmixing. An additional explanation could be an issue with the setup. The suspected issue in the setup causing this elongated tail is most likely located at the conductivity meter. The diameter of the tubing of the conductivity meter is very small in comparison to the diameter of the used tubing. This can result in an area of increased mixing at the connection of these two tubes resulting in an elongated E-curve. To verify this, a pulse experiment was performed where the monolithic reactor was replaced with a piece of tubing. The E(t) and E(θ) curve of this experiment are shown in Figure 31.

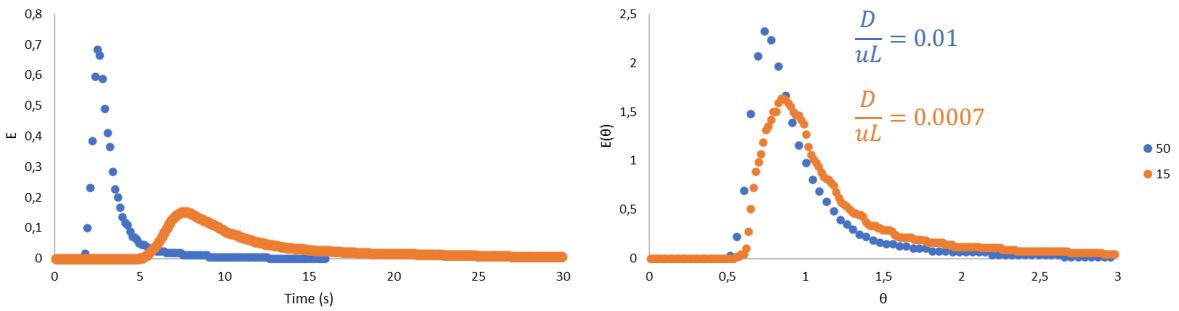

Figure 31: RTD experiment without translucent monolithic reactor at a flow rates of 15 ml/min (orange) and 50 ml/min (blue) E(t)-curves on the left and E(θ)-curves on the right.

In Figure 31 an elongated tail is still present, but the dispersion coefficients are smaller than 0.01 thus nearing plug flow. The elongated tail seems to get more noticeable at higher flow rates. as can be observed in the E(θ)-curves from both Figure 30 and Figure 31. Comparing the dispersion coefficients from Table 4 and Figure 31 it can be noted that there is a large deviation from plug flow when using the translucent monolithic reactor. The average dispersion coefficient here is 0.134. Therefore, it is hard to conclude if the suspected problem is an actual problem. To verify this, experiments could be conducted with another conductometer with a similar diameter to the tubing used.

A second observation in Figure 30 and Figure 31 is that at with an increased flow rate the peak comes before the observed average residence time. A logical explanation for this would be the increase of backmixing at higher flow rates. But looking at Table 4, no trend in the dispersion coefficients in function of the flow rate can be established supporting this explanation. Another logical explanation would be that at higher flow rates the chance of bypassing channels increases. But since in the E(θ)-curve θ is $t/\bar{t}_{observed}$ this explanation does not hold up either. Another explanation that comes to mind is the flow profile of the liquid at different velocities. All experiments are carried out in the laminar flow region. At higher flow rates (higher Reynolds number, more turbulent) the flow profile is more flattened compared to the flow profile at lower flow rates. Figure 32 illustrates an example of the influence of flow rate. At high flow rates this would result in a higher concentrated area that enters the conductometer first resulting in a steeper incline of concentration through time and thus an earlier peak.

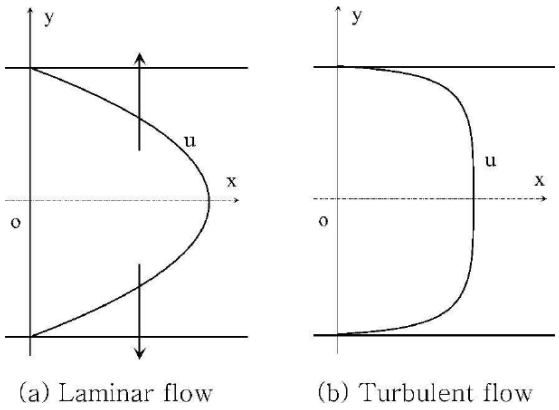

Figure 32: Flow profiles of laminar flow (a) and turbulent flow (b) [29]

A third and final observation is that the expected residence time generally matches the observed residence time from Table 4. A difference of the observed residence time being a couple

seconds smaller or larger than the expected one can be explained due to the volume of the setup not being considered in the calculation of the expected residence time and timing errors whilst carrying out experiments. For some experiments the observed residence time is much larger than the expected one e.g., monolith 3 at a flow rate of 5 ml/min. For this, no explanation is found. For other experiments e.g., monolith 2 and monolith 4 at a flow rate of 5 ml/min, the observed residence time is much smaller than the expected residence time. Both monoliths have the largest number of channels from the tested monolithic reactors. A likely explanation for this would be the occurrence of bypasses. In channels that are bypassed there is no flow resulting in a smaller reactor volume and thus a shorter observed residence time. These bypasses can occur when an air slug is present in that channel causing the pressure drop in that channel to be too high in comparison to other channels resulting in no flow through that channel. The fact that that this occurred at a low flow rate supports the explanation above since the pressure-drop within a channel increases with the increase of flow rate.

4.1.2.2. Optimal operating conditions

To determine the optimal operating conditions, the influence of a reflective background was tested for monolith 4. Also, the influence of the concentration of photosensitizer is studied. Finally, the optimal current to the LED was determined by comparing the influence of this parameter on the conversion, STY, and PSTY for monolith 1 and 4.

Reflective background and concentration of photosensitizer

Figure 33 illustrates the effect of the use of a reflective background for monolith 4 at different concentrations RB and shows the influence of the concentration photosensitizer.

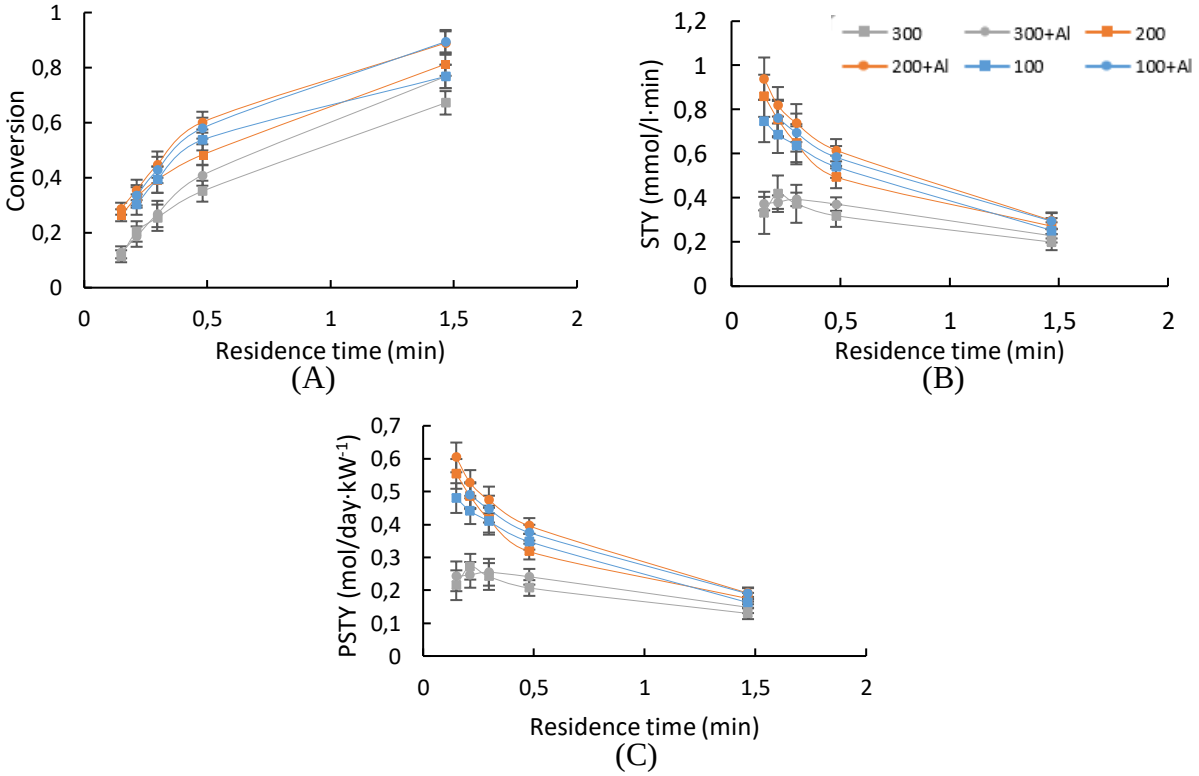

Figure 33: Plot of respectively the conversion (A), STY (B), and PSTY (C) in function of the residence time within the monolithic reactor 4 using a current of 0.3 A at concentrations of 100 µM (blue), 200 µM (grey), and 300 µM (orange) RB and with aluminum foil (•), and without aluminum foil (■).

From the graphs in Figure 33 it is clear that the addition of a reflective background results in a positive effect on the conversion, STY, and PSTY. At a concentration of 300 µM of RB the effects of the reflective background are slim. Also, the conversion, STY and PSTY at this concentration are the lowest out of all the experiments whilst having the highest concentration of photosensitizer. This can be explained by the assumption that more light is absorbed in the early channels allowing less light for the channels at the back of the monolith resulting in very low conversions in these channels and a minimal reflection of light by the background. This also results in a very low conversion at the back of the monolith. When the channels converge this will result in a lower conversion due to mixing of the reagents from each channel. When looking at the data at 200 µM and 100 µM the conversion, STY, and PSTY are near equivalent. This could be explained by the same effect. At a concentration of 200 µM more light is absorbed in the early channels with smaller amounts of light still reaching the back of the monolith. At a concentration of 100 µM less light is absorbed in the early channels allowing more light to reach the back of the monolith and then being reflected back to the channels. Due to the similar results a concentration of 100 µM RB is chosen as the optimal concentration for monolith 4.

Influence of current

Figure 34 illustrates the effect of the supply of different amounts of power by changing the current from 0.2 to 0.6 A to the LEDs for monolith 1 and 4 at a fixed flow rate of 15 ml/min.

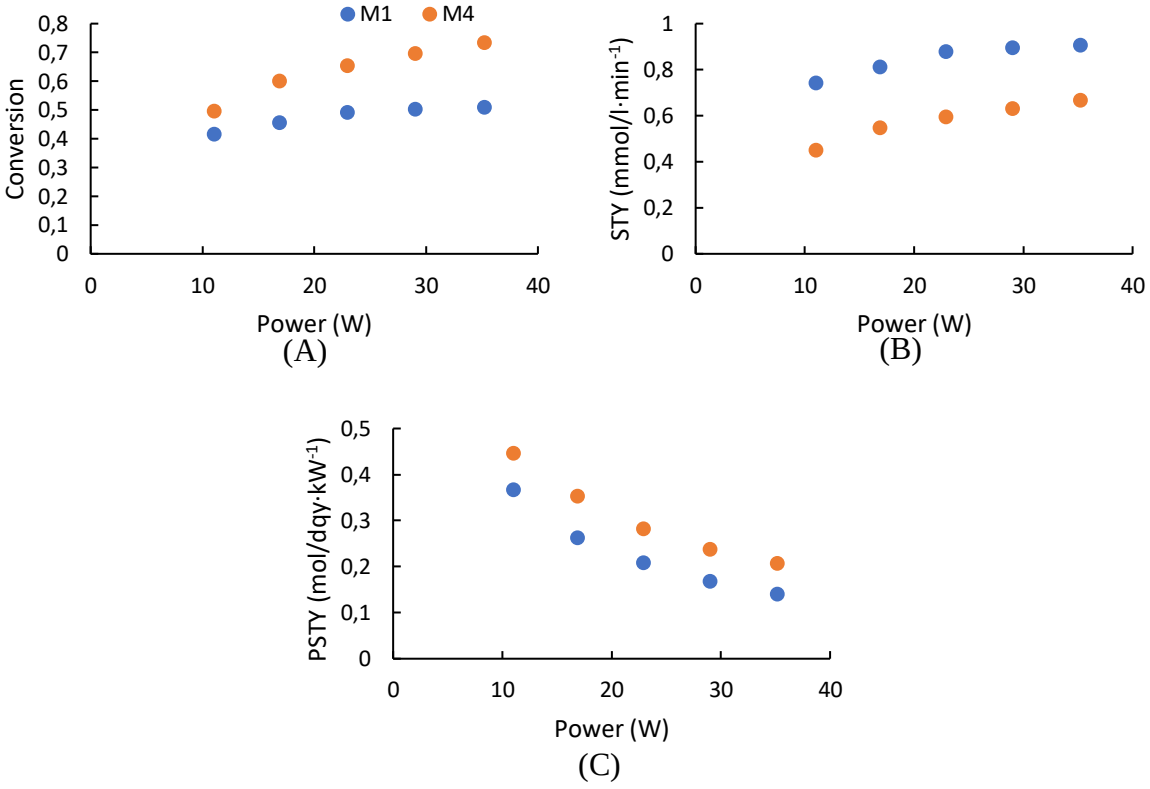

Figure 34: Plot of respectively the conversion (A), STY (B), and PSTY (C) in function of power supplied to the LEDs in monolithic reactor 1 (blue), and monolithic reactor 4 (grey).

Figure 34 reveals that an increase of current to the LEDs results in an increase of conversion, STY, and a decrease of PSTY. This trend can also be seen in Figure 29 at the results of the batch reactor. What stands out in in Figure 34 is the stagnation of conversion and STY at 24 W (current of 0.4 A) for monolith 1 and the decrease of the slope from this point on for monolith

4. When looking at the PSTY curve from this point on, it can clearly be seen that the PSTY keeps decreasing but with a smaller magnitude of slope with an increase of power to the LEDs. Due to the stagnation of STY and PSTY for monolith 1 and decrease of the slope for the STY and PSTY for monolith 4 at 0.4 A, this point is chosen as the optimal current where all four monoliths are compared.

Results for all monoliths

To compare all monoliths with each other, the dimensions and operating conditions of each monolith are needed. Table 5 shows the dimensions of the monolith and the parameters that were used for each monolith. The results regarding conversion, STY, and PSTY are shown in Figure 35.

Table 5: Dimensions of all four monolithic reactors and conditions that were used for the experiment

Monolith	Channels	Diameter	Current (A)	LEDs	Concentration RB (µM)
1	16x2	1	0.4	18	300
2	32x2	1	0.4	9	300
3	16x2	2	0.4	9	300
4	16x4	1	0.4	9	100

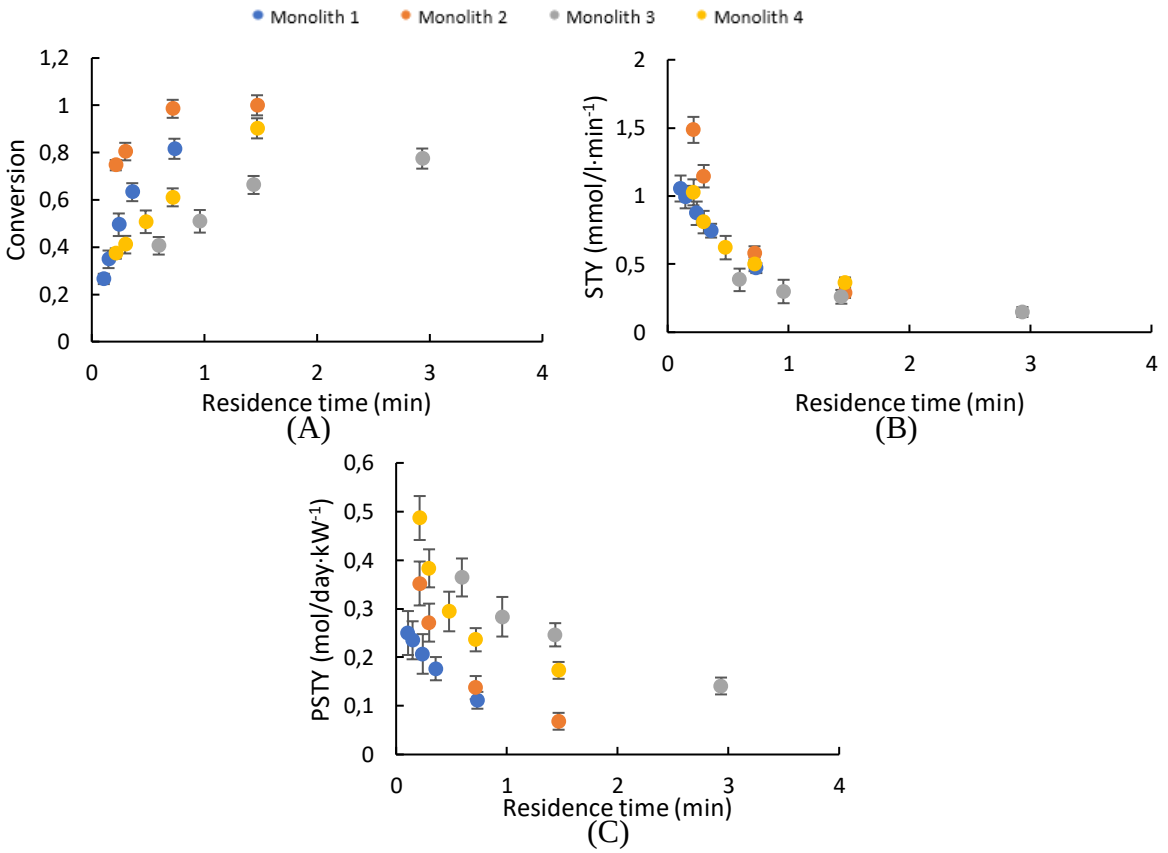

Figure 35: Plot of respectively the conversion (A), STY (B), and PSTY (C) in function of residence time in each translucent monolithic reactor, monolith 1 (blue), monolith 2 (orange), monolith 3 (grey), and monolith 4 (yellow)

Figure 35 reveals based on conversion and STY that monolith 2 outperforms the other monoliths. This is most likely explained by the larger number of LEDs that are used to irradiate the reactor compared to the other reactors. Monolith 2 is 32 channels wide whilst the other monoliths are 16 channels wide. This makes monolith 2 wider than the other monoliths allowing

the usage of more LEDs for irradiation. When comparing the PSTY of monolith 2 to the other monoliths, monolith 2 is not the most energy efficient out of the monoliths. What is interesting when comparing monolith 1 and 2 with each other is that monolith 2 is more energy efficient whilst using double the number of LEDs. Monolith 2 can be seen as two times monolith 1 glued next to each other. A probable explanation of this increase in efficiency is that the effect of the amounts of LEDs used outweighs the extra power used on the PSTY. Most likely due to the higher flowrate and conversion achieved in monolith 2 and at the same residence time as monolith 1. Another possible explanation is the effect of edging. An example of this effect is sketched in Figure 36.

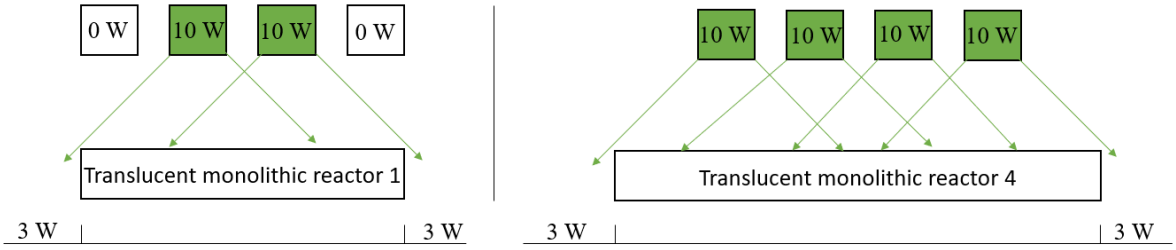

Figure 36: Sketch of the effect of edging with hypothetical values for power.

Edging is the effect of losing energy in the form of light at the side of the reactor because the light does not travel through the reactor. In this case a higher percentage of energy is lost at the edges of monolith 1 using 2 LED rows than at monolith 4 using 4 LED rows. This causes monolith 2 to have a higher ratio of used energy to the amount of total consumed energy. This effect could be studied by measuring the photon flux of light with a spectrophotometer in a straight horizontal line behind the monolith for both configurations. A comparison between the results should confirm whether this explanation is correct or not.

The results from monolith 3 regarding conversion and STY are the lowest out of all monoliths. A possible explanation for this is that this monolith did not receive enough light due to its large volume compared to the other monoliths. Furthermore, the larger channel size in the monolithic reactor results in a loss of the benefits from microchannels making problems of mass transfer limitations more likely to occur. This makes monolith 3 less suitable for multiphasic reactions.

Looking at the results of monolith 4 using monolith 1 as base result in Figure 35, it can be deduced that the placement of multiple sets of channels behind each other negatively effects the conversion and STY. In contrast, the PSTY is affected positively. A probable explanation of the positive effect on PSTY is the higher throughput that monolith 4 can accommodate in comparison with monolith 1. Resulting in a larger amount of moles reacted in the same period of time.

If the effect of edging is not the case, an interesting experiment that could be performed is making a monolith that is double as wide as monolith 4 by increasing the number of channels from 16x4 to 32x4 and performing the reaction with double the number of LEDs. The effect that is expected is the same as seen in the difference between monolith 1 and 2 that are discussed above.

4.2. Multi-phase (G/L)

4.2.1. Steps towards slug flow

The first attempt to achieve gas-liquid slug flow was with water and air. Here flow rates between 0-50 ml/min for both gas as liquid were tested. The observed result was that almost all flow went through a select number of channels with a result that there was no flow in other channels and thus a bypass was created. This could be visualized by slugs in those channels not moving and with the addition of a dye, no color change was observed in the stationary channels. This observation could be explained by the increase of pressure drop caused by an air slug that was too high relative to the pressure drop in other channels making flow in those channels stop. The pressure drop of a gas slug can be estimated with the Laplace equation given in equation 12 and it is dependent on the surface tension (σ) and the diameter of the slug d_{slug}. In micro-channels, liquids with a high surface tension can block the branch channels [30].

$$\Delta P_{slug} = \frac{\sigma \cdot 2}{d_{slug}} \tag{12}$$

The second attempt to achieve slug flow was with the use of a surfactant to decrease the surface tension of the liquid phase making the pressure drop of a slug decrease. In this experiment it was observed that in the first few seconds of the experiment a uniform slug flow is achieved but after a this most of the air flow travelled through a couple of channels. There still was flow within those other channels. But this flow was primarily single phase. Another issue with the use of surfactants is the formation of unwanted foam.

The third experiment was almost identical to the second. The only difference is that a thin tube with a diameter of 0.57 mm with a length of 30 mm is added after the monolith. This is done to add an extra pressure drop in the hope that the slugs would distribute evenly over the entire monolith. This resulted in no significant difference compared to experiment 2. It can most likely be concluded that the pressure drop of this small thin tube was not high enough. But for safety reasons higher pressures are not tested because connections between different tube-sizes and the connection with the monolith was done with flexible tubing that cannot withstand high pressures without coming loose/leaking.

The foam caused by the solution using surfactant and water is still an issue. To solve this issue another solvent is used in experiment four with similar properties to water but with a lower surface tension. This solvent was ethanol. The results of the experiments were comparable to these of experiment 2 but without the foam. Making ethanol the solvent that is chosen to continue with.

To further decrease the pressure-drop of each slug within monolithic reactor. The sixth experiment was done in a squared-channel monolithic reactor. In circular channels the liquid film thickness is thinner than the film thickness in square channel [31]. This thinner film thickness causes for the gas-slug to have a higher shear resulting in a higher pressure-drop caused by a slug. Here, the start up is very promising with equal slug sizes and velocities in all channels but after a short period of time the system becomes unstable. Resulting in unequal G/L distributions for each channel where some channels receive no gas or even show a reversed flow direction.

Gas-liquid up-flow is always unstable and that a slight increase of gas flow into a channel decreases the liquid hold-up in that channel. Creating a slight underpressure at the bottom entrance of the channel which in turn draws even more bubbles into the channel [32]. This explains the obtained results from experiments one to six. Therefore, the seventh experiment is similar to experiment six. For experiment seven, the flow direction is changed from up-flow to down-flow. Here the opposite trend to up-flow is observed. In the beginning the flow pattern is unstable with only gas flow through a couple of channels. After a short period of time the slug flow stabilizes. Resulting in a uniformly spread slug flow over each channel. At first the slug flow was not consistent due to the use of a pulsating pump. By changing this pump to a constant syringe pump there was a consistent slug flow, but the velocity varies from channel to channel. When the combined flow rate of the gas and liquid is too low, the slug flow was unstable. This is a logical observation and can be explained by the low pressure drop in the channels at low flow rates. Here the gravitational force exceeds the resistance the channels causing an uneven distribution of the gas-liquid mixture resulting in flow only going through select channels. Varying the liquid to gas ratio a lower ratio resulted in larger air slugs in relation to the size of the liquid slugs. A good ratio for slug flow that was experimentally determined was 50/50. To determine the velocity in each channel for different runs the PIVLab extension in Mathlab was used. Figure 37 shows the velocity profiles of this experiment at a total gas/liquid flow rate of 35 ml/min.

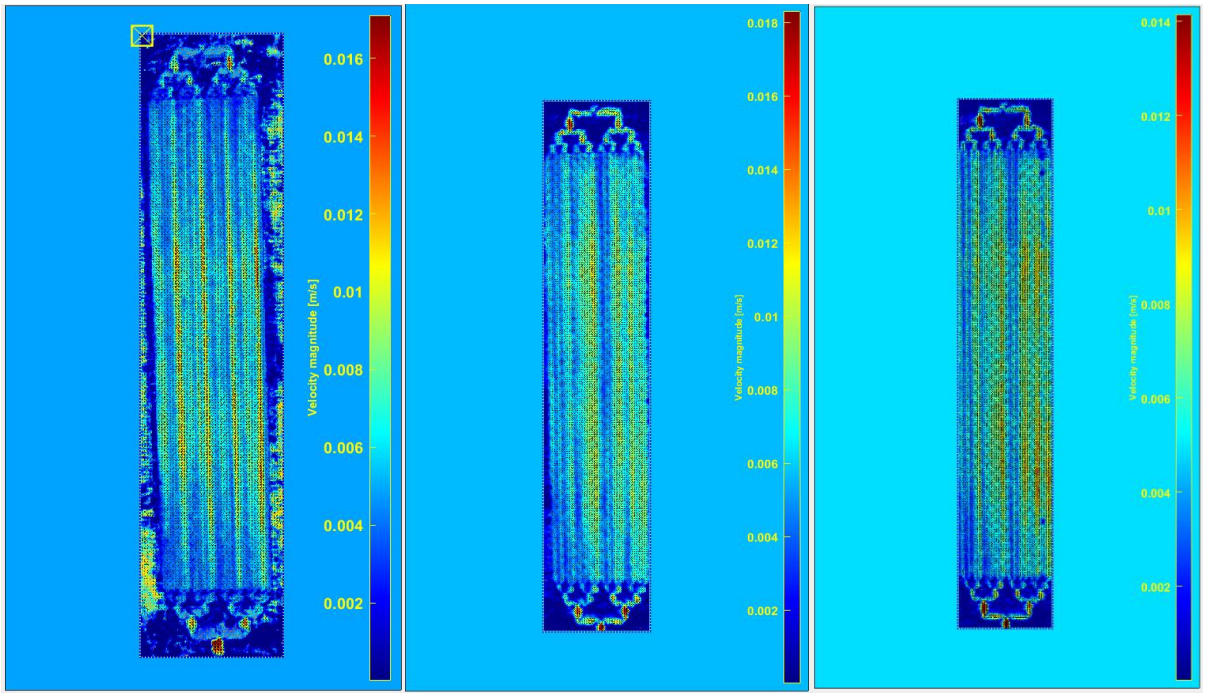

Figure 37: Velocity profile images obtained using PIVLab

Figure 37 reveals that there is no significant difference between the obtained results. All three runs have similar velocity profiles. So, it can be concluded that the slug flow is similar for each run. When looking at the velocities on the profile, it seems like there is barely any flow in some channels compared to others and the velocity of the slugs is lower than expected. This is not the case, and the issue most likely originates from a combination of factors such as reflections, camera angle, size/number of slugs in a channel, and interference of slugs in underlying channels. To explain this in more detail, the basics of how PIVLab processes data needs to be

explained. PIVLab registers movement by comparing the video frame by frame and looking at changes of color from each and correlating this to vectors. This means that only the borders between liquid and air slugs are registered. When there is a lot of reflection possibly caused by a bad camera angle, not all borders of the slugs will be detected and movement in the reflection will be measured. This causes inaccuracies and interferences in the velocity profile. This is also the case with underlying channels. A bad camera angle can also cause a gradient in velocities due to stretching of the images. When the slugs are larger (less slugs in a channel), there will be a smaller number of vectors in that channel due to the smaller number of borders between the liquid and gas-phase resulting in a lower average measured velocity.

To verify whether slug flow with just water or water with surfactant is achievable in the downwards flow direction. These liquids are also tested in experiment eight. The experiment with water resulted in similar results as the experiments with water and upwards flow. The experiment with water and 0.08 M SDS resulted in similar results as experiment seven but still with the issue of the formation of foam.

The ninth and final experiment that is performed is with a gas to liquid ratio of 1 and with a total flow rate of 30 ml/min. This experiment attempts to get rid of reflections and interference of underlying channels but keeping these channels present. This is done by recording the video in an area with less light and by designing a slit into the monolith where a piece of paper can be put in between to cover up the underlying channels. The velocity profile obtained from PIVLab is shown in Figure 38.

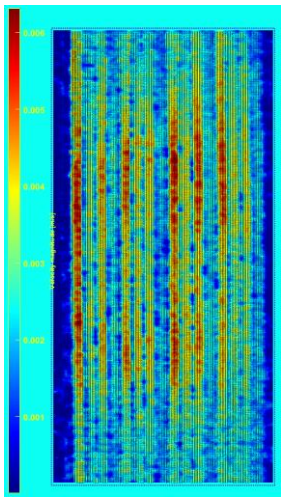

Figure 38: Velocity profile image obtained using PIVLab

In Figure 38 the velocity decreases from the middle to the edges. This is not the case since the velocity though a channel stays constant. The change in observed velocity is most likely caused by the stretch of the image due to these points being further away from the camera lens resulting in optical distortion. Another recurring observation is with the velocities calculated using PIVLab. The velocity near the center of the monolith is according to Figure 38 near 0.6 cm/s. When calculating the expected velocity, the velocity of the mixture in a channel should be around 1.56 cm/s. Therefore, the velocity within each channel was calculated manually. An average velocity of 1.76 cm/s was found. The difference between the velocity achieved from PIVLab and the expected & calculated can be explained by the way that PIVLab processes data as mentioned above. In short, PIVLab only detects movement at the areas where a colour

transition is present. This means that only the edges of a slug are measured, and the rest of the slug has no velocity. Taking an average of the velocity of all the processed frames causes a dilution of the velocity in the velocity profiles. Because of this, PIVLab cannot be used to correctly create an accurate speed profile for slug flow within the entire monolithic reactor at once. To do this, all recorded vectors from all frames should be placed onto a single profile which is not yet possible using PIVLab.

4.2.2. Multiphase reaction

To perform the multiphasic reaction, it was attempted to achieve slug flow using ACN instead of ethanol because all reactions are done in ACN. This would give comparable results for single phase and multiphase. In this attempt it was clear that the use of ACN was not suitable to obtain slug flow due to the formation of bypasses for the gas-phase. Therefore, the gas/liquid-phase reaction is carried out in ethanol. Due to the use of a different solvent, a new calibration curve is needed using ethanol as solvent. The calibration curve is shown in Figure 39.

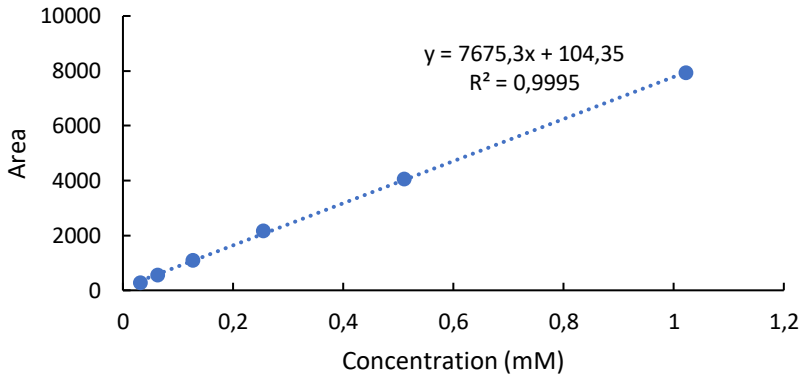

Figure 39: Calibration curve of DPA in ethanol

For the multiphasic reaction of DPA a conversion of 0.22 is obtained. At this conversion the STY equals 0.80 mmol/l·min^{-1} and the PSTY equals 0.48 mol/day·kW^{-1}. Since these results are obtained using ethanol as the solvent instead of ACN it is difficult to compare the obtained results to these of single-phase. This is because the solvent influences parameters such as the lifespan of a singlet oxygen molecule [33].

4.3. Comparison of reactors

To objectively compare the obtained results from the translucent monolithic reactor such as STY, PSTY (at a specific conversion) at least three criteria must be met. The first criterion is that both reactors use the same model reaction. When using different model reactions parameters such as solubility or reactivity of the molecule influence the reaction rate. The second one is that reaction is performed in the same solvent. The solvent influences the lifespan of a singlet oxygen molecule. When the lifespan is longer, singlet oxygen has more time to find a molecule to react with. This usually results in a higher productivity [33]. The third criterion is that the reaction is performed in the same phase system. In this case a single-phase system. The fourth and final criterion that is discussed here, is that that a similar performing photosensitizer must be used.

In literature two reactors are found that meet these first three criterion. The photosensitizer that is used for both reactions is Methylene Blue. The first reactor is the fluorescent fluid photochemical microreactor (FFPM). The FFPM is a microreactor with multiple parallel channels. The best results that were obtained in this study was with 8 channels having a serpentine design as shown in Figure 40. Based on available data given in [32, Fig. 4] a STY of 0.058 mmol/l·min^{-1} was obtained at a conversion of 0.77 and a flow rate of 1.64 ml/min. The value of the PSTY was 0.022 mol/day·kW^{-1}. To calculate this value the consumed power of the LED used in the study was estimated at 9.5 W [34].

The second reactor is a luminescent solar concentrator-based photomicroreactor (LSC-PM). The design of this LSC-PM is similar to the design used in this thesis. The difference is that the LSC-PM only consists out of one row of channel while the tested translucent monolithic reactors consist out of 2 to 4 rows of channels. The best results that were obtained in this study was with 32 channels as shown in Figure 40. Based on available data given in [33, Fig. 10] a STY of 0.18 mmol/l·min^{-1} was obtained at a conversion of 0.83 and a flow rate of 0.37 ml/min. The PSTY could not be calculated due to the limited data available on the used light source [35].

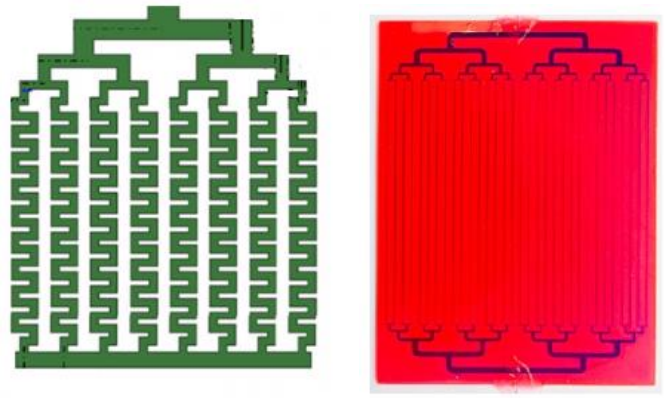

Figure 40: Image of the reactors that are used to compare against the translucent monolithic reactor FFPM (on the left) and LSC-PM (on the right)

To compare the obtained data from literature to the translucent monolithic reactors, a diagram that displays the STY, PSTY, and at what flow rate the reactor reached a conversion near 0.8. This diagram is displayed in Figure 41 is set up.

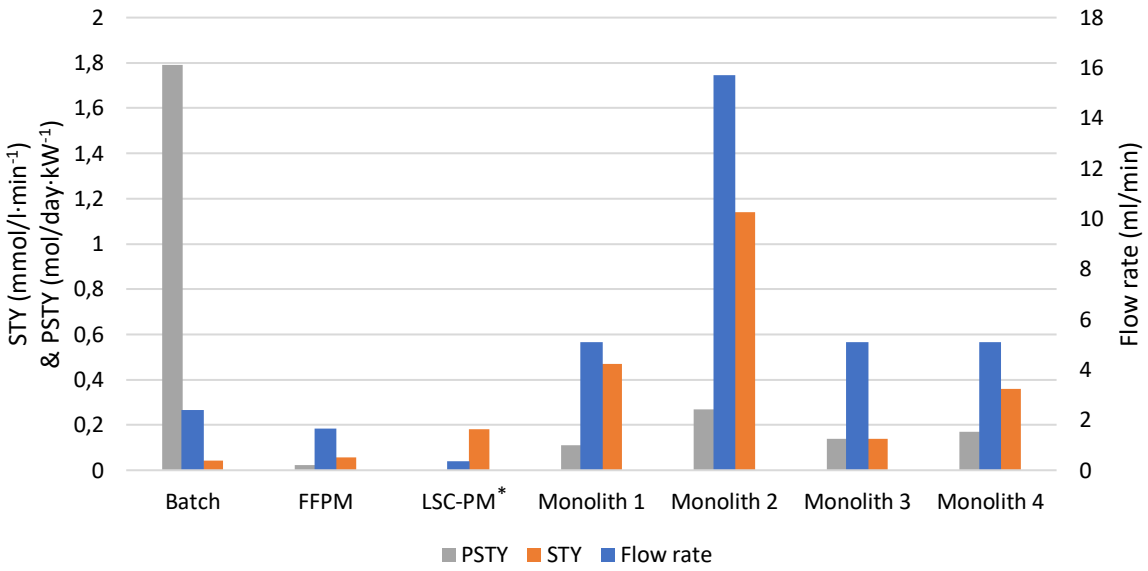

Figure 41: bar diagram used to compare the Batch, FFPM, and LSC-PM to the translucent monolithic reactor based on STY, PSTY, and flow rate at a conversion near 80%. * For the LSC-PM no PSTY value could be obtained/calculated*

As previously stated in the comparison between the translucent monolithic reactors, translucent monolithic reactor 2 performs the best out of the tested translucent monolithic reactors. Therefore, monolithic reactor 2 is compared to the batch reactor, FFPM, and LSC-PM. From the data presented in Figure 41, it can be concluded that in the comparison of monolith 2 to the batch reactor the batch reactor is 6.6 times more energy efficient but 26 times less productive. Compared to the FFPM, monolith 2 is more productive and energy efficient with a STY being 20 times larger and the PSTY 13 times larger. Finally, in the comparison with the LSC-PM it can be noted that monolith 2 is 6.3 times as productive as the LSC-PM.

It should be noted that the translucent monolithic reactor is only compared to other microreactors due to the scarcity of comparable data found in literature. From this it can be concluded that the translucent monolithic reactor seems to be a promising scalable reactor but to come to a rock-solid conclusion how the reactor places against its competitors. It would be interesting to obtain comparable data of other size comparable photoreactors to compare to.

5. Conclusion and Future work

5.1. Conclusion

The main goals of this thesis are met. The translucent monolithic reactor is compared to other photochemical reactors at a conversion of 80%. These reactors are the batch reactor, FFPM, and LSC-PM. Translucent monolithic reactor 2 performed the best out of the translucent monolithic reactors being more productive than the other three reactors with the STY of 1.14 $mmol/l \cdot min^{-1}$ being respectively 26-, 20-, and 6.3-times larger than this of the batch reactor, FPM, and LSC-PM. Regarding the energy efficiency, the PSTY of the translucent monolithic reactor is 0.27 $mol/day \cdot kW^{-1}$ being 6.6 times smaller than this of batch reactor and 13-times larger than this of the FFPM. It must be noted that in this study the translucent monolithic reactor was only compared to the batch reactor and two other scale-up design flow reactors and not to a reactor with an equal throughput. This is because no comparable data was found in literature.

Also, slug flow is achieved in the translucent monolithic reactor with square channels. The achieved slug flow is not identical for each channel with each channel having differences in velocities and the slugs within each channel not having identical sizes. In the steps towards achieving slug flow, it became clear that parameters such as the pressure drop within each channel of the translucent monolithic reactor are key in characterizing slug flow within the translucent monolithic reactor. The pressure drop within each channel must be close to identical for each channel to obtain an identical slug flow pattern for each channel.

5.2. Future work

It would be interesting to study whether the effect of edging is the explanation for the improved performance of monolith 2 compared to monolith 1. Also, to compare the current state of the reaction in gas/liquid slug flow to the single-phase reaction. The single-phase reaction must be performed in ethanol at a similar residence time. It would be interesting to see what the effect of the currently obtained multiphasic system is on the conversion, STY, and PSTY. Furthermore, there is still work to characterize and optimize slug flow within the translucent monolithic reactor. After slug flow has been characterized the translucent monolithic reactor could be compared to other multiphase photochemical reactors

References

[1] K. Loubière, M. Oelgemöller, T. Aillet, O. Dechy-Cabaret, and L. Prat, "Continuous-flow photochemistry: A need for chemical engineering," *Chem. Eng. Process. Process Intensif.*, vol. 104, pp. 120–132, 2016, doi: https://doi.org/10.1016/j.cep.2016.02.008.

[2] G. Mul, T. Van Gerven, and A. Stankiewicz, "Reactors Using Alternative Energy Forms for Green Synthetic Routes and New Functional Products," *Nov. Concepts Catal. Chem. React. Improv. Effic. Futur.*, pp. 289–308, 2010, doi: 10.1002/9783527630882.ch13.

[3] C. Sambiagio and T. Noël, "Flow Photochemistry: Shine Some Light on Those Tubes!," *Trends Chem.*, vol. 2, no. 2, pp. 92–106, 2020, doi: 10.1016/j.trechm.2019.09.003.

[4] D. Cambié, C. Bottecchia, N. J. W. Straathof, V. Hessel, and T. Noël, "Applications of Continuous-Flow Photochemistry in Organic Synthesis, Material Science, and Water Treatment," *Chem. Rev.*, vol. 116, no. 17, pp. 10276–10341, 2016, doi: 10.1021/acs.chemrev.5b00707.

[5] M. B. Plutschack, B. Pieber, K. Gilmore, and P. H. Seeberger, "The Hitchhiker's Guide to Flow Chemistry," *Chem. Rev.*, vol. 117, no. 18, pp. 11796–11893, 2017, doi: 10.1021/acs.chemrev.7b00183.

[6] M. Jacobs, E. Kayahan, L. C. J. Thomassen, S. Kuhn, and M. E. Leblebici, "First generation of translucent monoliths for photochemical applications," *J. Adv. Manuf. Process.*, vol. 2, no. 2, pp. 1–11, 2020, doi: 10.1002/amp2.10047.

[7] K. N. Loponov, J. Lopes, M. Barlog, E. V. Astrova, A. V. Malkov, and A. A. Lapkin, "Optimization of a scalable photochemical reactor for reactions with singlet oxygen," *Org. Process Res. Dev.*, vol. 18, no. 11, pp. 1443–1454, 2014, doi: 10.1021/op500181z.

[8] M. Pape, "Industrial applications of photochemistry," *Pure Appl. Chem.*, vol. 41, no. 4, pp. 535–558, 1975, doi: 10.1351/pac197541040535.

[9] M. E. Leblebici, "Design, modelling and benchmarking of photoreactors and separation processes for waste treatment and purification," KU Leuven, 2017.

[10] K. G. McKendrick, *Principles and Applications of Photochemistry*, vol. 36, no. 9. 1989.

[11] L. Thys, "Photodegradation of diclofenac in the first generation of translucent monoliths," UHasselt & KU Leuven, 2020.

[12] E. Wieërs and S. Wouters, *Fysica voor industrieel ingenieurs deel 2*. Diepenbeek: UHasselt/KULeuven, 2014.

[13] "File:Emwavepropagation.jpg - CleanEnergyWIKI." http://cleanenergywiki.org/index.php?title=File:Emwavepropagation.jpg (accessed Sep. 07, 2020).

[14] "File:EM spectrum.svg - Wikimedia Commons." https://commons.wikimedia.org/wiki/File:EM_spectrum.svg (accessed Sep. 07, 2020).

[15] J. Silverman *et al.*, "Radiation physics," *Britannica*. 2021, [Online]. Available: https://www.britannica.com/science/radiation.

[16] J. Llorca, "Monolithic Reactor BT - Encyclopedia of Membranes," E. Drioli and L. Giorno, Eds. Berlin, Heidelberg: Springer Berlin Heidelberg, 2015, pp. 1–3.

[17] O. Levenspiel, *Chemical reaction engineering*, Third., vol. 38, no. 11. John Wiley & Sons, 1999.

[18] V. A. Atiemo-Obeng and R. V. Calabrese, *Rotor–Stator Mixing Devices*. 2004.

[19] "photosensitization," in *IUPAC Compendium of Chemical Terminology*, Research Triagle Park, NC: IUPAC.

[20] M. C. DeRosa and R. J. Crutchley, "Photosensitized singlet oxygen and its applications," *Coord. Chem. Rev.*, vol. 233–234, pp. 351–371, 2002, doi: 10.1016/S0010-8545(02)00034-6.

[21] D. B. Min and J. M. Boff, "Chemistry and reaction of singlet oxygen in foods," *Compr. Rev. Food Sci. Food Saf.*, vol. 1, no. 2, pp. 58–72, 2002, doi: 10.1111/j.1541-4337.2002.tb00007.x.

[22] L. Zhang *et al.*, "Fluorescent Fluid in 3D-Printed Microreactors for the Acceleration of Photocatalytic Reactions," *Adv. Sci.*, vol. 6, no. 13, pp. 1–6, 2019, doi: 10.1002/advs.201900583.

[23] E. Adaze, A. Al-Sarkhi, H. M. Badr, and E. Elsaadawy, "Current status of CFD modeling of liquid loading phenomena in gas wells: a literature review," *J. Pet. Explor. Prod. Technol.*, vol. 9, no. 2, pp. 1397–1411, 2019, doi: 10.1007/s13202-018-0534-4.

[24] C. Franco and J. 3rd Olmsted, "Photochemical determination of the solubility of oxygen in various media.," *Talanta*, vol. 37, no. 9, pp. 905–909, Sep. 1990, doi: 10.1016/0039-9140(90)80251-a.

[25] F. A. Holland and R. Bragg, "7 - Gas–liquid two-phase flow," F. A. Holland and R. B. T.-F. F. for C. E. (Second E. Bragg, Eds. Oxford: Butterworth-Heinemann, 1995, pp. 219–267.

[26] M. E. Leblebici, G. D. Stefanidis, and T. Van Gerven, "Comparison of photocatalytic space-time yields of 12 reactor designs for wastewater treatment," *Chem. Eng. Process. Process Intensif.*, vol. 97, pp. 106–111, 2015, doi: 10.1016/j.cep.2015.09.009.

[27] "B for Biology: Spectrophotometry - UV-Visible Spectrophotometry." http://namrataheda.blogspot.com/2013/07/spectrophotometry-part-2-uv-visible.html (accessed Sep. 07, 2020).

[28] S. Czaplicki, "Chromatography in Bioactivity Analysis of Compounds," in *Column Chromatography*, Intech., 2013, pp. 99–122.

[29] H.-S. Dou, "Energy Gradient Theory of Hydrodynamic Instability," Jan. 2005.

[30] Y. Liu, W. Sun, and S. Wang, "Experimental investigation of two-phase slug flow distribution in horizontal multi-parallel micro-channels," *Chem. Eng. Sci.*, vol. 158, pp. 267–276, 2017, doi: https://doi.org/10.1016/j.ces.2016.10.021.

[31] R. S. Patel, J. A. Weibel, and S. V Garimella, "Characterization of liquid film thickness in slug-regime microchannel flows," *Int. J. Heat Mass Transf.*, vol. 115, pp. 1137–1143, 2017, doi: https://doi.org/10.1016/j.ijheatmasstransfer.2017.08.008.

[32] M. T. Kreutzer, F. Kapteijn, J. A. Moulijn, and J. J. Heiszwolf, "Multiphase monolith reactors: Chemical reaction engineering of segmented flow in microchannels," *Chem. Eng. Sci.*, vol. 60, no. 22, pp. 5895–5916, 2005, doi: https://doi.org/10.1016/j.ces.2005.03.022.

[33] R. H. Young, K. Wehrly, and R. L. Martin, “Solvent effects in dye-sensitized photooxidation reactions,” *J. Am. Chem. Soc.*, vol. 93, no. 22, pp. 5774–5779, Nov. 1971, doi: 10.1021/ja00751a031.

[34] Z. Zhu, L. Yang, Y. Yu, L. Zhang, and S. Tao, “Scale-up Design of a Fluorescent Fluid Photochemical Microreactor by 3D Printing,” *ACS Omega*, vol. 5, no. 13, pp. 7666–7674, Apr. 2020, doi: 10.1021/acsomega.0c00511.

[35] F. Zhao *et al.*, “Scale-up of a Luminescent Solar Concentrator-Based Photomicroreactor via Numbering-up,” *ACS Sustain. Chem. Eng.*, vol. 6, no. 1, pp. 422–429, 2018, doi: 10.1021/acssuschemeng.7b02687.